Theory of Self-Assembled Bilayers Near a Cylindrical Hydrophobic Insertion

Theory of Self-Assembled Bilayers Near a Cylindrical Hydrophobic Insertion

By

Michael Donald Birch, B.Sc. (Honours)

A Thesis

Submitted to the School of Graduate Studies

in Partial Fulfilment of the Requirements

for the Degree

Master of Science

McMaster University

Master of Science (2016) McMaster University

(Department of Physics and Astronomy) Hamilton, Ontario

TITLE: Theory of Self-Assembled Bilayers Near a Cylindrical Hydrophobic Insertion

AUTHOR: Michael Birch, B.Sc. (Honours)

SUPERVISOR: Dr. An-Chang Shi

NUMBER OF PAGES: viii, 84

Abstract

We develop a coarse-grained model of lipids and proteins in which the lipids are modelled as diblock copolymers and the proteins as rigid cylinders. The generic protein model allows the possibility of amphipathic proteins with intrinsic curvature. Self-consistent field theory (SCFT) is used to determine the morphology of the lipid bilayer in the vicinity of the proteins. In particular, we focus on the case of a long transmembrane protein inserted perpendicular to the bilayer. For this system we use SCFT to determine the mechanical properties of the membrane and the thickness profile as a function of distance from the protein inclusion. The mechanical constants are also used in an elastic theory to predict the thickness profile. Good agreement between the full SCFT and elastic theory is obtained. We also use SCFT to determine systematic trends of the boundary conditions for the thickness profile at the protein interface. Such results could be used as boundary conditions for the description of bilayers using elastic theory. We show that this system undergoes a second order wetting transition as the interaction strength between the protein and membrane is varied.

Acknowledgements

I am grateful to my supervisor, Dr. An-Chang Shi, for his guidance and encouragement during this project. Thanks as well to (soon to be Dr.) Ashkan Dehghan for always being willing to answer my questions and provide advice. I also owe thanks to Dr. Ben Bolker for improving my skills in the R programming language. This allowed me to write a much better code for use in this work than I would have been able to otherwise.

I would also like to thank my friends and family for helping to keep me sane during the stressful times of graduate school.

Table of Contents

List of Figures

Chapter 1

Introduction

1.1 Lipid Bilayers and Proteins

1.1.1 Types of Lipids and Bilayer Composition

Lipids are amphiphilic molecules which self-assemble in aqueous environments to form many different structures, in particular they can form bilayer membranes [1]. Such membranes are the structural basis for many living organisms and may have been important for the evolution of life itself [2, 3]. Cellular membranes are characterized as a "fluid mosaic", in which the various components of the membrane, including proteins, can diffuse laterally along the surface formed by the lipid bilayer [4]. This fluid structure leads to many interesting mechanical properties, which will be discussed later. In order to maintain the stability of the fluid membrane, several different types of lipid molecules are required [5], which will be discussed briefly in what follows.

Lipid molecules can differ from one another in terms of their hydrocarbon tail length (i.e. number of carbons in the tail) and saturation (i.e. number

of carbon-carbon double bonds). These properties of the lipids (in addition to others not discussed here) determine the geometry of their self-assembled structure [6]. The most abundant type of lipids in the plasma membrane of cells are those which spontaneously form flat (zero spontaneous curvature) bilayers, for example phosphatidylcholine (PC) [7]. Lipids of this type can be thought of as having a cylindrical shape, in which the head group and tail group have approximately equal volumes [8]. See Figure 1.1a.

For other types of lipids, the tail group can take up more or less volume than the head group. Such lipids do not necessarily self-assemble into flat bilayers because of their asymmetric structure and instead form morphologies with some spontaneous curvature [6]. For example, phosphatidylethanolamine (PE) is a lipid in which the tail group has a larger area than the head group and hence has more of a conical shape [8], see Figure 1.1b. Conversely, lipoprotein(a) (LPA) has a small tail group compared to its head group. Thus LPA has an inverse conical shape [8], see Figure 1.1c. Due to the intrinsic curvatures of the structures which conical and inverse conical lipids form on their own, these lipids are associated with stabilizing negative and positive curvatures, respectively [8, 9].

Cellular membranes contain lipids of all three types along with many different proteins and constitute a complex system. Interactions in this system include those between the different types of lipids with the proteins [10, 11], interactions between the different types of lipids between themselves [4, 8, 9], indirect interactions between proteins via the lipids [12] and interactions of the membrane with other cellular components [4]. During this work we will not

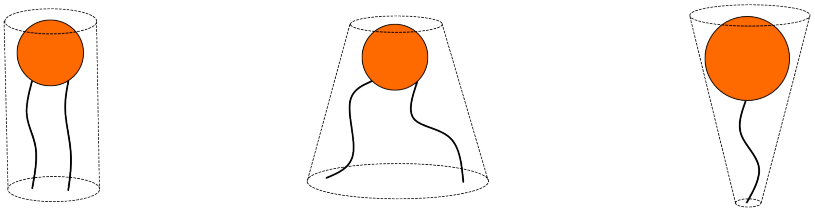

(a) Cylindrical (zero spontaneous curvature) lipid, e.g. PC.

(b) Conical (negative spontaneous curvature) lipid, e.g. PE.

(c) Inverse conical (positive spontaneous curvature) lipid, e.g. LPA.

Figure 1.1: Schematic of different lipid types.

consider this full range of complexity, but rather focus on a few key aspects of the membranes and use models which adequately capture those features. In the following subsections we will present the motivation behind the aspects of membrane biophysics which were studied in this work.

1.1.2 Mechanical Properties of Lipid Bilayers

The idea that lipid bilayers could be modelled by a continuum-mechanical description was proposed by Canham, Helfrich and Evans, all around the same time [13–15]. This idea turned out to be extremely fruitful in terms of understanding the various shapes which membranes can have [16, 17]. Their main insight was that at the macroscopic level (so that the membrane can be treated as a 2D surface), the energy associated with the shape of the membrane must depend on parameters which describe that shape. Thus they connected lipid

bilayers with differential geometry. In particular, Helfirch considered a free energy functional of the form [16]

$$F = \int dA \left(\frac{1}{2} k_b (2H + c_0)^2 + \overline{k} K + \gamma \right), \tag{1.1.1}$$

where k_b is the bending modulus, H is the mean curvature, c_0 is the spontaneous curvature, $\overline{k}$ is the Gaussian bending modulus, K is the Gaussian curvature, and γ is the surface tension. The mean curvature, H, is the average of the two principle curvatures, while the Gaussian curvature, K, is their product. The principle curvatures are the curvature (reciprocal of the radius of curvature) in each of the two independent directions one could move on the surface. For example, on a cylinder the two directions are up/down the length and around the circular cross-section. The former has zero curvature, while the later has curvature given by $1/R$, where R is the radius of the cylinder. Thus, for a cylinder $H = 1/2R$ and $K = 0$.

The bending moduli and surface tension are mechanical properties of the membrane. They depend only on the membrane composition and not its shape[a], hence these constants are useful descriptors for differentiating and characterizing membranes. For this reason, significant experimental and theoretical efforts have been made in measuring and making use of these properties (see e.g. [16, 17, 19]).

[a] The independence of the mechanical constants is only approximately true. One can think of Equation 1.1.1 as an expansion of the free energy up to second order in the curvature and hence only gives a good description for small curvatures, while vary large curvatures could require higher-order terms. However, as the curvature becomes larger the radius of curvature shrinks, and once this length scale is on the order of bilayer thickness, such a continuum description would no longer be valid [18].

Our interest in these constants lies in investigating the consistency of elastic theory and self-consistent field theory (SCFT). Elastic theories are based on Helfrich's free energy functional and require the mechanical properties as input. On the other hand, self-consistent field theory is a meso-scale theory from which the mechanical constants can be determined. Hence, we can take the mechanical properties of the bilayer determined by SCFT and make predictions about the bilayer shape using elastic theory. However, such predictions about the shape can also be made within SCFT itself. If the two theories are consistent then these predictions should agree. In this work we show the consistency of SCFT with elastic theory in this way (see section 4.2).

1.1.3 Transmembrane Proteins and Hydrophobic Mismatch

Cellular membranes, while structurally based on lipid bilayers, contain other components, such as proteins. Proteins in the cell membrane perform crucial tasks, such as transport of materials across the membrane and signalling [20]. They are also targeted by many drugs [21]. Thus studying the interactions of these proteins with the cell membrane is important for future drug development. The study of these proteins is also relevant to detection and treatment of certain membrane based disease, for example Alzheimer's disease [22].

Most membrane proteins span the thickness of the membrane [21], connecting the inside of the cell to the outside. Such proteins are called "transmembrane proteins." It has been observed that the same membrane can accommodate transmembrane proteins of various lengths and the same trans-

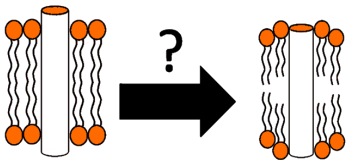

Figure 1.2: Schematic of how the lipids may stretch in order to accommodate hydrophobic mismatch.

membrane protein can be found in membranes of different thicknesses [23]. We define "hydrophobic mismatch" to be the difference between the length of the hydrophobic core of the transmembrane protein (often an α-helix) and the hydrophobic thickness of the membrane in which the protein is embedded. Hydrophobic mismatch is energetically unfavourable since the protein could be too long (positive hydrophobic mismatch), causing the hydrophobic section to be in contact with the polar solvent. Alternatively, the hydrophobic section is too short (negative hydrophobic mismatch), causing the hydrophilic section of the protein to be in contact with the membrane's hydrophobic core [24]. In order to accommodate positive or negative hydrophobic mismatch lipids may stretch (as in Figure 1.2) or compress, respectively. However, there is an entropic cost to stretching or compressing the lipid tails in order to remove the mismatch completely since fewer configurations are available to a polymer which has been stretched or confined. Therefore, the optimal configuration of the lipids near a transmembrane protein is a non-trivial balance between these two contributions to the free energy.

In this work we focus on positive hydrophobic mismatch, using a protein which is much longer than the membrane thickness. The reason for this is computational simplicity, however it is not a significant limitation of the work

and in fact provides an opportunity to study an additional phenomenon. For values of the protein-membrane interaction which are not too large, the membrane will stretch a finite amount and the remaining protein length will not impact the bilayer morphology, thus the system becomes essentially equivalent to one with a finite length protein. However, for large enough values of the membrane-protein interaction, the membrane will completely wet the protein. While the later case is not relevant in a biological context, this wetting phase transition does have interesting physics (see subsection 1.3.2). Results related to the transmembrane system are presented in chapter 4.

1.1.4 Membrane Curvature and Proteins

The use of differential geometry, specifically the curvature of surfaces, has been useful in studying the shape of membranes. On the other hand, membrane proteins perform many important biological functions. There is also evidence that these two ideas are in fact related through so-called "curvature sensing" and "curvature generating" proteins [25]. Curvature sensing occurs when a protein will preferentially bind to regions of the membrane with a particular curvature, while curvature generation occurs when a protein locally reshapes the membrane to have a particular curvature. The two phenomena are distinguished based on whether the protein changes the membrane (as in curvature generating) or not. The interactions of proteins with membrane curvature and its biological relevance has been the focus of many experimental and theoretical studies in recent years (see Refs. [11, 25–34] and references therein).

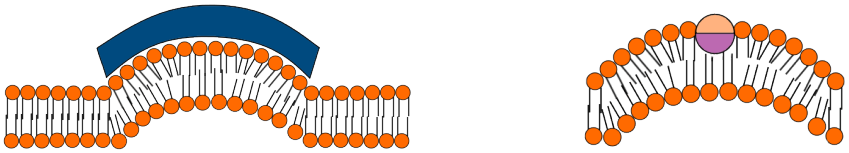

(a) Scaffolding (b) Amphipathic insertion

Figure 1.3: Schematic of curvature sensing/generating mechanisms.

There are several proposed mechanisms by which curvature sensing and generating could occur. The two mechanisms which will be discussed in this work are scaffolding and amphipathic insertion. Scaffolding occurs when a surface-bound protein has some intrinsic curvature [31] (e.g. BAR proteins [32]), while amphipathic insertion involves a protein which embeds itself halfway into the membrane since half of the protein (divided along the long axis) is hydrophobic and the rest is hydrophilic [28]. These two mechanisms are represented schematically in Figures 1.3a and 1.3b, respectively.

One of the original goals of this work was to investigate the circumstances under which a protein will sense or generate curvature. This is an important question since it is known that the two phenomena are related and that some biological processes use curvature as a control mechanism, for example in clathrin coated pit formation [35]. The theoretical framework to answer this question is developed in chapter 2, however the numerical difficulties arising from the implementation of our model discussed in subsection 3.3.3 have prevented further progress.

1.2 Previous Theoretical Studies

The present work is not the first to investigate the ideas and phenomena presented in the previous section. Here we briefly outline some of the previous theoretical and computation works in this area and how the present work builds on them.

1.2.1 Molecular Dynamics Simulations

Molecular dynamics (MD) simulations are considered the computational method closest to reality for investigating complicated systems which are governed by classical mechanics [19, 36]. The advantage of these simulations is that great molecular detail could be included, thus making use of our detailed knowledge of the chemical structure of many biologically relevant proteins and lipids. However, the disadvantage is the great computational cost of including such detail. For this reason, MD simulations are limited in terms of the size of systems which can be investigated as well as the time-scale on which the systems can be observed. As an example of a typical study, MD was used to investigate the epsin-ENTH domain in a system composed of $\sim 10^6$ particles and simulated behaviour on time scales of $\sim 1 - 100$ ns [37]. Recent advances in computing have allowed larger system to be investigated, even approaching experimental length scales [38], thus reducing this limitation.

In spite of these limitations, MD simulations are considered to be a standard against which other models can be tested since few phenomenological parameters are needed [36]. Comparisons between MD and more phenomenological models can help us elucidate what essential features of the system

reproduce the behaviour of interest, thus contributing to our mechanistic understanding of these complex systems. While we do not directly compare our results with any MD simulations, we do compare with and validate elastic theory, which is often used in conjunction with MD simulations in order to extract mechanical properties of bilayers. This is done by fitting the thermal fluctuation spectra obtained in the MD simulation to the spectrum predicted by elastic theory [19, 36, 39]. In this work we verify the parameters obtained in such a fit are indeed physically meaningful, hence validating the approach.

1.2.2 Elastic Theories

We have already mentioned the importance of elastic theory to the study of membranes in subsection 1.1.2. Here we will focus on one work in particular, that of Tjörnhammar and Edholm [40]. In this work, the authors use the free energy functional

$$F[t] = \frac{1}{2}\iint dxdy \ \left(k_s \left|t - t_0\right|^2 + \gamma \left|\nabla t\right|^2 + k_b \left|\nabla^2 t\right|^2\right), \tag{1.2.1}$$

to describe how the thickness of a membrane is affected by hydrophobic mismatch. In Equation 1.2.1 $t(x, y)$ is the thickness, k_s is the stretching modulus (in the direction normal to the bilayer), γ is the surface tension and k_b is the bending modulus. In their work they define the length scale $\xi = (k_b/k_s)^{1/4}$ to non-dimensionalize the system. Applying the Euler-Lagrange equation to Equation 1.2.1 in cylindrical coordinates (assuming rotational symmetry), we obtain an equation for $\tilde{t}(r) = t(r) - t_0$,

$$\rho^3 \tilde{t}^{(4)} + 2\rho^2 \tilde{t}''' - (1 - \gamma_0 \rho^2)\left(\rho \tilde{t}'' - \tilde{t}'\right) + \rho^3 \tilde{t} = 0, \tag{1.2.2}$$

where $\rho = r/\xi$ and $\gamma_0 = \gamma/\sqrt{k_b k_s}$. The authors then solve Equation 1.2.2 with $\gamma_0 = 0$, subject to suitable boundary conditions, in order to make general conclusions about the shape of the thickness profile. They then tried to validate their theory by comparing with MD simulations, however the mechanical properties which enter their theory are not directly accessible by experiment and so values of k_s and k_b are chosen by a combination of assumptions relating them to other parameters and fitting to simulation data.

Validating elastic theories by fitting parameters as opposed to determining them directly according to their physical interpretation is a common practice (e.g. see Refs. [41–43]). This raises the question as to whether the parameters of these theories carry the physical meaning we believe they do, or if they are simply phenomenological parameters which parametrize a family of curves that happen to fit well to simulations or experiments. In this work we answer this question in the following way. First we determine the mechanical constants directly within our theoretical framework (see subsection 2.2.3). Second, we compare the elastic theory profiles, obtained from those constants, with the predictions made by the same theoretical framework used to determine the bilayer properties. Thus, we directly test the consistency of elastic theory with our own.

1.2.3 Self-Consistent Field Theory

Finally, we include, for completeness, a brief discussion of previous works which employed Self-Consistent Field Theory (SCFT) since that is the theoretical framework which is also applied here. SCFT can be thought of a

mesoscopic theoretical tool which bridges the gap between MD and elastic theory. This is because SCFT does not include molecular detail (results are average concentrations of the various chemical species) like MD, however does contain more detail than a continuum description. In addition to being conceptually in between the two other theoretical tools, it is also mid-way in terms of computational difficulty. SCFT is not nearly as computationally expensive as an MD simulation, however is certainly more costly than solving a differential equation (or several) numerically.

While several SCFT studies concerning bilayer membranes have been done previously [18, 44–46], to the best of our knowledge, only one other SCFT work concerns bilayer membranes and proteins. This is the work by Kik *et al.* [47] and also considered the problem of hydrophobic mismatch, as well as made comparisons with predictions by elastic theory. However, their work, while similar to what is done here, is distinct from ours. The differences lie in the formulation of the theory (their discrete formulation versus our continuous one) and the bilayer properties studied (they studied area per lipid while we study bilayer thickness). In addition, the elastic theory Kik *et al.* use for comparison is different from that used here. Therefore, we view the previous work as complimentary to our own.

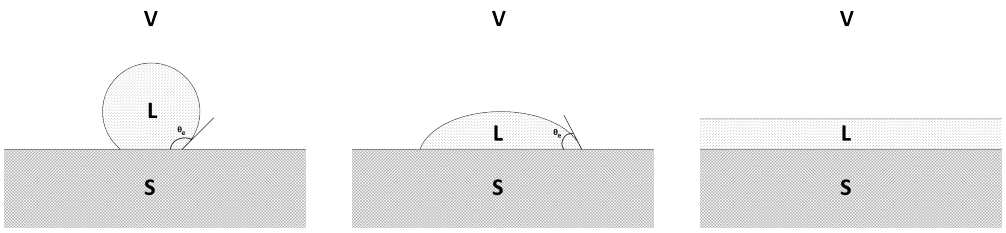

(a) Partial wetting with $\theta_e > 90°$.

(b) Partial wetting with $\theta_e < 90°$.

(c) Complete wetting ($\theta_e = 0°$).

Figure 1.4: Schematic of partial and complete wetting.

1.3 Wetting Phase Transitions

1.3.1 General Theory

Classically, wetting is thought of in terms of a liquid drop on a solid substrate in equilibrium with its vapour. The greater affinity the liquid has for the substrate, the more favourable it will be to have greater surface area of the drop in contact with the substrate and hence the more "wetted" the surface will be. The limiting case of very high affinity is complete wetting, in which the liquid forms a uniform layer on the entire substrate surface. Situations in which some wetting occurs, but not complete wetting, are called partial wetting. The degree to which the surface is wetted can be quantified by the wetting angle, θ_e, which is defined to be angle between the substrate and the inner liquid surface. The smaller θ_e, the more the surface is wetted, with $\theta_e = 0$ corresponding to complete wetting. See Figure 1.4 for diagrams of different wetting scenarios. A wetting phase transition is then defined as the transition between the partial and complete wetting phases.

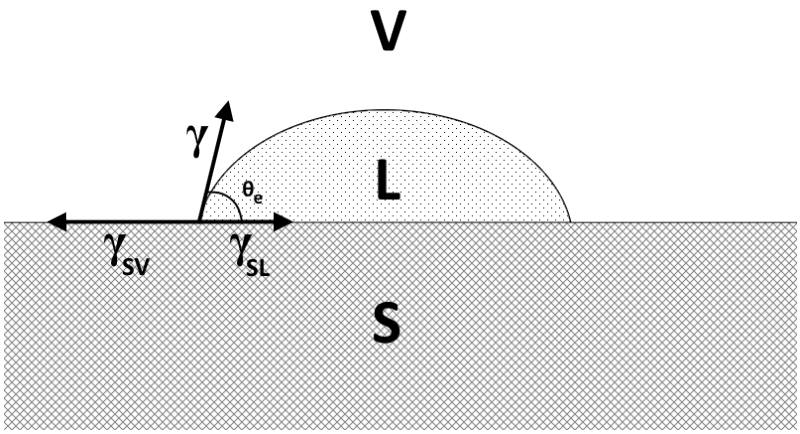

Figure 1.5: Diagram explaining Young's formula.

The wetting angle can be related to physical properties of the system via Young's equation [48]

$$\gamma_{SV} - \gamma_{SL} - \gamma \cos\theta_e = 0, \tag{1.3.1}$$

where γ_{SV}, γ_{SL} and γ are the interfacial tensions of the solid-vapour, solid-liquid and liquid-vapour interfaces respectively. One way in which to understand this relationship is by thinking of the surface tensions as forces, then Young's relation is simply the statement that the forces at the point where the three phases meet must sum to zero since the system is in equilibrium (see Figure 1.5).

One of the simplest, yet most successful theoretical descriptions of wetting transitions is the Cahn model [48]. This is a continuum model; which includes only short-range interactions and can be used to calculate how the various system surface tensions change with temperature. Thus, using Young's formula, the Cahn model can predict when wetting will occur. This model also predicts that both first and second order wetting transitions are possible, with the for-

mer occurring when there is a discontinuous jump in the density of the fluid at the substrate surface and the latter occurring when a microscopic thickness film continuously grows into one of macroscopic thickness.

1.3.2 Wetting in Polymer Systems

While temperature is the parameter used in Cahn's model, polymer systems can exhibit wetting transitions by varying other parameters. In particular, the strength of the interaction between different chemical species in the system (parameterized by Flory-Huggins parameters, see subsection 2.2.2)[b] can be used [49]. It has been seen previously that Cahn-like second order wetting transitions can occur in polymer systems by varying one Flory-Huggins parameter, while keeping the others fixed [49].

In the system we are interested in here, the substrate is a cylindrical hydrophobic insertion through a bilayer membrane, the membrane itself is the wetting fluid and the parameter we vary is the the membrane-protein interaction (Flory-Huggins parameter). As discussed in subsection 1.1.3, this system can be used to model transmembrane proteins, however the motivation for looking for a wetting transition is not biological since such wetting of proteins has not been observed in cellular membranes. Instead, this part of our study is motivated by the interesting physics this system presents, as well as finding an

[b] Varying these parameters could still be thought of as changing the temperature since interaction strength between polymers does change with temperature. However, we want to make it clear that we are directly changing the Flory-Huggins parameter and hence that is the parameter we will focus on.

upper bound for the membrane-protein interaction beyond which the system no longer has biological relevance.

The interesting physics of exploring a wetting transition of a bilayer membrane on a hydrophobic surface arises from the fact that, unlike with a droplet of simple liquid, the spreading of the bilayer across the substrate depends not only on surface tension, but also on the energies associated with stretching the membrane from its preferred thickness and with bending the membrane as this stretching occurs. This bending energy becomes especially important in the complete wetting phase since the resulting structure in that case has a sharp kink, which connects the monolayer forming the wetting layer to the main bilayer membrane. The results of this study are given in section 4.1.

Chapter 2

Model System

2.1 Lipids as Diblock Copolymers

As discussed in subsection 1.1.1, the key property of lipids which cause them to self-assemble into bilayer membranes is that they are amphiphilic, i.e. they are composed of hydrophilic and hydrophobic components. Diblock copolymers are molecules which consist of two polymer chains, each composed of chemically distinct monomer species, covalently bonded together. Therefore, diblock copolymers could also act as amphiphilic molecules and hence would capture the essential property of lipids. Different types of lipids were distinguished based on the relative size of the head and tail groups (c.f. Figure 1.1). These differences between lipids can also be captured by diblock copolymers through changing the relative lengths of the two polymer chains which compose the diblock. Let N_A be the number of monomers in the chain of species A (here assumed to be modelling the lipid head group) and N_B be the number of monomers in the chain of species B. Then $N_A = N_B$ would correspond to a lipid with no intrinsic curvature, i.e. cylindrical lipid shape. While

$N_A < N_B$ and $N_A > N_B$ would correspond to the conical and inverse conical lipid shapes, respectively. Indeed, evidence supporting this correspondence has been found in the qualitative agreement between theory and experiment in the recent work published by Dehghan *et al.* [50].

Since plasma membranes are primarily composed of cylindrical-type lipids, our model should use primarily symmetric diblock copolymers. In fact, since this work deals only with small curvatures, we will simplify the system and only include symmetric diblock copolymers. Since conical and inverse conical lipids tend to aggregate in regions of high curvature [50], including only cylindrical lipids should not impact the results of our low-curvature system.

Having motivated the use of diblock copolymers as a model of lipid molecules, in what follows we present the theoretical tools which have been developed to study the morphology of diblocks.

2.2 Self-Conistent Field Theory

2.2.1 Gaussian Chain Model

The Gaussian Chain Model is one of the simplest continuum chain models which captures the basic properties of linear polymers. Despite its simplicity, when this model is applied to diblock copolymers, the resulting self-assembled structures have been found to be accurately reproduce the structural properties of lipid membranes [44]. Here we present the basic assumptions and results

of this model necessary for the development of Self-Consistent Field Theory (SCFT). This discussion is based on that given in Ref. [51].

To begin, we assume that the chain is composed of N statistical units. Each unit has a random length, but all lengths are sampled from the same distribution. The mean length of a statistical segment is b. When applying this model to a particular real polymer, N and b are often chosen such that the average arclength, Nb, and the mean square end-to-end distance (defined below) are equal to the values for the real polymer. In that case b is called the Kuhn length.

The backbone of the polymer is described by the space curve, $\mathbf{r}(s)$, $s \in [0, N]$, where $\mathbf{r}(s)$ gives the position of the s-th unit. We assume that each unit is statistically independent of each other in terms of both length and direction, i.e. $\langle \mathbf{r}'(s) \cdot \mathbf{r}'(t) \rangle = b^2 \delta(s-t)$, where $\langle \cdot \rangle$ represents an ensemble average over possible polymer chains and δ is the Dirac delta function. Notice that this requirement gives the average arclength of the backbone to be $\left\langle \int_0^N ds \ \|\mathbf{r}'(s)\| \right\rangle = Nb$, as stated above. Moreover, the mean square end-to-end distance, defined as $R_{\text{ee}}^2 = \left\langle \|\mathbf{r}(N) - \mathbf{r}(0)\|^2 \right\rangle$, can be computed as

$$\begin{aligned} R_{\text{ee}}^2 &= \left\langle \left\| \int_0^N ds \ \mathbf{r}'(s) \right\|^2 \right\rangle \\ &= \left\langle \int_0^N \int_0^N ds dt \ \mathbf{r}'(s) \cdot \mathbf{r}'(t) \right\rangle \\ &= Nb^2. \end{aligned}$$

A similar calculation shows that the radius of gyration, defined as the root mean square distance of a segment from the centre of mass of the chain is given by $R_g = b\sqrt{N/6}$.

Finally, we assume that the bonds between segments of the chain can be thought of as linear springs. The potential energy is thus

$$\frac{U[\mathbf{r}(s)]}{kT} = \frac{3}{2b^2}\int_0^N ds \ \left\|r'(s)\right\|^2, \tag{2.2.1}$$

where k is Boltzmann's constant and T is the temperature. This assumption is valid as long as the real polymer is not forcefully stretched so far the the shape of the true bond potential (often modelled as a Lennard-Jones potential) becomes important and cannot be approximated as being simply quadratic. Using standard Maxwell-Boltzmann statistics, the probability of observing a chain is a particular configuration is proportional to the Boltzmann factor, given by

$$p[\mathbf{r}(s)] \propto \exp\left(-\frac{3}{2b^2}\int_0^N ds \ \left\|r'(s)\right\|^2\right). \tag{2.2.2}$$

2.2.2 SCFT for AB/C Polymer Blends

We now present the Self-Consistent Field Theory (SCFT) for a blend of AB-diblock copolymers with C-homopolymers. Here we only give some notation and results, leaving the details of the derivation to Appendix A.

Let n_1 diblock copolymer and n_2 homopolymer chains be in a volume V. Let N_1, N_2 be the total degree of polymerization of the diblock and homopolymer chains respectively. Let $N_\alpha = f_\alpha N_1$, where $\alpha \in \{A, B\}$ give the number of A- and B-type monomers in the diblock respectively. Since we are applying the continuous Gaussian chain model (see subsection 2.2.1), we must define a statistical length for each monomer type, $b_\alpha = \sigma_\alpha b$, where $\alpha \in \{A, B, C\}$ and b is a reference statistical length. We will also choose the diblock copolymer as the

reference degree of polymerization, $N = N_1$, and define $\kappa_p = N_p/N,\ p \in \{1, 2\}$ so that $\kappa_1 = 1$ and $\kappa_2 = \kappa$. Recall from subsection 2.2.1 that the radius of gyration for a polymer with degree of polymerization N and statistical length b is $R_g = b\sqrt{N/6}$. This will be the adopted length scale used in the calculations. We will assume that both polymers have the same monomer density, ρ_0, which is defined as the number of monomers per unit volume. The "hardcore" volume, i.e. the space taken up by one monomer which cannot be occupied by more than one monomer, is thus ρ_0^{-1}. In SCFT we do not keep track of individual molecules, but instead consider the ensemble average concentration of each species at each point in space. The hard-core interactions are captured in this formalizm by demanding that the system be incompressible, i.e. the sum of the concentrations of all the chemical species at each point in space is equal to unity. Given the definitions thus far, the spatial average concentration of each polymer type is

$$\overline{\phi_p} = \frac{n_p N_p}{\rho_0 V}, \tag{2.2.3}$$

where $p \in \{1, 2\}$.

As mentioned above, SCFT works with ensemble average concentrations (which can vary from point to to point in space), $\phi_\alpha(\mathbf{r}), \alpha \in \{A, B, C\}, r \in V$. Along with these concentrations are average local chemical potential fields, $\omega_\alpha(\mathbf{r})$, which capture interactions between the different chemical species. Naturally, the potential fields depend on the concentrations since the interactions at each point in space will depend on what polymers are present at that point. However, the concentrations also depend on the potentials since potential gradients would cause polymers to move. There is one other field which is

needed in characterizing the system, the pressure (or incompressibility) field, $\eta(\mathbf{r})$. Mathematically, this field is a Lagrange multiplier which enforces the incompressibility constraint mentioned above. However, physically it can be interpreted as the local pressure felt by the monomers at that point due to hard-core interactions. In SCFT we are looking for the equilibrium configuration, i.e. the set of fields $\{\phi_\alpha, \omega_\alpha, \eta\}$ such that the potential and pressure fields produced by the concentrations would not change those concentrations.

The above paragraph can be formalized by using statistical mechanics to write a free energy functional in terms of the various fields,

$$f\left[\{\phi_\alpha\},\{\omega_\alpha\}\right] = \frac{1}{V}\int d\mathbf{r}\left(\frac{1}{2}\sum_{\alpha\neq\beta}\chi_{\alpha\beta}N\phi_\alpha(\mathbf{r})\phi_\beta(\mathbf{r}) - \sum_\alpha \omega_\alpha(\mathbf{r})\phi_\alpha(\mathbf{r})\right) - \sum_p \frac{\overline{\phi_p}}{\kappa_p}\ln\mathcal{Q}_p, \tag{2.2.4}$$

where $\chi_{\alpha\beta}$ are Flory-Huggins parameters, which give the strength of the interaction between species α and β (negative values is attraction, positive values are repulsion) and $\mathcal{Q}_p$ are defined below. The goal of finding an equilibrium set of fields corresponds to finding a local minimum of the free energy functional. Using functional differentiation, one obtains the following mathematical relationships between the concentrations, potentials and pressures:

$$\phi_\alpha(\mathbf{r}) = \frac{\overline{\phi_1}}{\mathcal{Q}_1}\int_0^{f_\alpha} q_\alpha(\mathbf{r},s)q_\alpha^\dagger(\mathbf{r},f_\alpha-s)\,ds,\ \alpha\in\{A,B\} \tag{2.2.5}$$

$$\phi_C(\mathbf{r}) = \frac{\overline{\phi_2}}{\kappa_2\mathcal{Q}_2}\int_0^{\kappa_2} q_C(\mathbf{r},s)q_C(\mathbf{r},\kappa_2-s)\,ds \tag{2.2.6}$$

$$\omega_\alpha(\mathbf{r}) = \sum_{\alpha\neq\beta}\chi_{\alpha\beta}N\left(\phi_\beta(\mathbf{r}) - \overline{\phi_\beta}\right) + \eta(\mathbf{r}) \tag{2.2.7}$$

$$\sum_{\alpha\in\{A,B,C\}}\phi_\alpha(\mathbf{r}) = 1, \tag{2.2.8}$$

where $\mathcal{Q}_1$ and $\mathcal{Q}_2$ are functionals of the fields $\omega_\alpha(\mathbf{r})$, since the functions q_α and $q_\alpha^\dagger$ depend on $\omega_\alpha(\mathbf{r})$,

$$\mathcal{Q}_1\left[\{\omega_\alpha\}\right] = \frac{1}{V}\int q_A^\dagger(\mathbf{r}, N_A)\ d\mathbf{r} = \frac{1}{V}\int q_B^\dagger(\mathbf{r}, N_B)\ d\mathbf{r} \tag{2.2.9}$$

$$\mathcal{Q}_2\left[\omega_C\right] = \frac{1}{V}\int q_C(\mathbf{r}, N_C)\ d\mathbf{r}. \tag{2.2.10}$$

The functions q_α and $q_\alpha^\dagger$ satisfy the following modified diffusion equation with initial conditions:

$$\frac{\partial q_\alpha}{\partial s} = \sigma_\alpha^2\nabla^2 q_\alpha - \omega_\alpha q_\alpha,\ \ \alpha \in \{A, B, C\} \tag{2.2.11}$$

$$q_\alpha(\mathbf{r}, 0) = 1 \tag{2.2.12}$$

$$\frac{\partial q_\alpha^\dagger}{\partial s} = \sigma_\alpha^2\nabla^2 q_\alpha^\dagger - \omega_\alpha q_\alpha^\dagger,\ \ \alpha \in \{A, B\} \tag{2.2.13}$$

$$q_\alpha^\dagger(\mathbf{r}, 0) = q_\beta(\mathbf{r}, f_\beta),\ \ \beta \neq \alpha. \tag{2.2.14}$$

Notice that Equation 2.2.7 and Equation 2.2.8 define a linear relationship between the potential fields and the concentration/pressure fields and can be written in matrix form as

$$\begin{bmatrix} \omega_A \\ \omega_B \\ \omega_C \\ 0 \end{bmatrix} = \begin{bmatrix} 0 & \chi_{AB}N & \chi_{AC}N & 1 \\ \chi_{AB}N & 0 & \chi_{BC}N & 1 \\ \chi_{AC}N & \chi_{BC}N & 0 & 1 \\ 1 & 1 & 1 & 0 \end{bmatrix} \begin{bmatrix} \phi_A - \overline{\phi_A} \\ \phi_B - \overline{\phi_B} \\ \phi_C - \overline{\phi_C} \\ \eta \end{bmatrix}. \tag{2.2.15}$$

Equation 2.2.15 can be used to obtain an explicit expression for η in terms of $\{\omega_\alpha\}$. One could therefore define a loop for updating the potential and pressure fields as follows:

Algorithm 2.2.1. `Input:` $\{\omega_\alpha\}$, η

1. Solve Equation 2.2.11 and Equation 2.2.13
2. Compute $\mathcal{Q}_1$ and $\mathcal{Q}_2$ using Equation 2.2.9 and Equation 2.2.10
3. Compute $\{\phi_\alpha\}$ using Equation 2.2.5 and Equation 2.2.6
4. Compute the new potential fields, $\{\omega'_\alpha\}$, using Equation 2.2.7
5. Compute the new pressure field, η', by solving Equation 2.2.15 with $\{\omega'_\alpha\}$ on the L.H.S.

If the updated fields, $\{\omega'_\alpha\}$ and η' are the same as the input fields within some tolerance then a self-consistent solution has been found.

2.2.3 Determining Mechanical Properties of Membranes Within SCFT

As mentioned in subsection 1.2.2, the elastic theories describing the deformation of a membrane require mechanical properties of the leaflets of the bilayer (i.e. a monolayer) as input. Using SCFT we can determine those properties and hence compare the predictions of SCFT with elastic theories directly. The elastic theory we focus on the most is that of Tjörnhammar and Edholm [40], which has a free energy functional given by

$$F[t] = \frac{1}{2}\iint dxdy\ \left(k_s\left|t-t_0\right|^2 + \gamma\left|\nabla t\right|^2 + k_b\left|\nabla^2 t\right|^2\right), \tag{2.2.16}$$

where $t(x,y)$ is the thickness of the membrane. The first term represents the energy cost for stretching the membrane from its natural thickness, t_0, while the second and third terms are the costs associated with surface tension and

bending the membrane, respectively. Therefore, we wish to determine the three mechanical constants associated with stretching, k_s, surface tension, γ, and bending, k_b, using SCFT.

The stretching modulus can be determined directly by fitting a quadratic function to the free energy as a function of $|t - t_0|$ for a flat membrane. The membrane thickness can be measured directly from the concentration profiles in the SCFT solution and it can be changed by simply changing the box size used in the numerical implementation of SCFT. It is important to note that Equation 2.2.4 is a free energy per unit volume per chain and includes not only the bilayer, but also the bulk solution in which the bilayer sits. Therefore, in order to properly compare with Equation 2.2.16, the quantity we need to use is $V(f - f_{\text{bulk}})$, where V is the volume of system, f is given by Equation 2.2.4 and f_{bulk} is the free energy per unit volume per chain of the bulk surrounding the bilayer. Then k_s (in units of free energy per chain per length-squared) can be determined by fitting the coefficients of

$$V(f - f_{\text{bulk}}) = \frac{1}{2} A k_s \left|t - t_0\right|^2 + F_0, \tag{2.2.17}$$

where A is the area of the bilayer and F_0 is a constant giving the free energy of a flat membrane with its natural thickness. In fact, the constant F_0 also gives the surface tension, γ, of the membrane, $F_0 = \gamma A$. This is because the only deviations of f from the bulk value in the case of a flat membrane with the natural thickness result from the interfaces which define the membrane and surface tension is simply the energy per unit area of an interface.

Finally, we need to also determine the bending modulus, k_b. This is done using the method presented by Matsen [52]. This method uses cylindrical

coordinates in 1D in order to bend the monolayer in a controlled way and thus determine the bending modulus. Using cylindrical coordinates in 1D forces the membrane to bend into a cylindrical conformation (i.e. a tube). By varying the radius of this tube we can control how much bending occurs (or more preciously, the curvature of the bilayer). The result is that k_b can be determined by fitting the coefficients of

$$V(f - f_{\text{bulk}}) = \frac{1}{2} A k_b C^2 + F_0, \tag{2.2.18}$$

where $C = 1/R$, is the curvature of the monolayer (R is the radius of the monolayer in the cylindrical coordinate system).

2.3 Proteins as Masks

2.3.1 General Formulation

To include a protein into the SCFT formalism we use a technique called "masking" [53]. In this method we include additional concentration fields in the SCFT equations called masks. These masks take up space (due to the incompressibility condition) and can interact with the polymers in the system (by including additional terms in Equation 2.2.7). Thus, masking allows us to determine how the polymer system will interact with an external object within SCFT. Generally, we think of the masks as being specified in advance (similar to boundary conditions of a partial differential equation), and we solve the SCFT equations for the polymer fields around them. However, it is possible to have the masks change in response to the polymers as well. This is done by

fixing the mask fields, finding polymer fields which satisfy the SCFT equations, then changing the masks to respond to that polymer fields SCFT solution and repeating until the mask fields no longer change (i.e. are in equilibrium with their associated SCFT solution polymer fields solution). This has been done previously, for example in work on nanoparticles suspended in polymer solutions [54].

Specifically, for our system, we can suppose that the protein mask is composed of two parts: ϕ_V and ϕ_W, corresponding to the hydrophilic and hydrophobic parts, respectively. The SCFT equations given in subsection 2.2.2 then change as follows. Equation 2.2.8 (the incompressibility condition) becomes

$$\phi_A + \phi_B + \phi_C + \phi_V + \phi_W = 1 \tag{2.3.1}$$

and Equation 2.2.7 becomes

$$\omega_\alpha(\mathbf{r}) = \sum_{\beta \neq \alpha} \chi_{\alpha\beta} N \left(\phi_\beta(\mathbf{r}) - \overline{\phi_\beta} \right) + \eta(\mathbf{r}), \ \alpha \in \{A, B, C\}, \ \beta \in \{A, B, C, V, W\}. \tag{2.3.2}$$

The structure of Algorithm 2.2.1 is unchanged by these modifications so long as we assume ϕ_V and ϕ_W are fixed. We will consider in more detail how to handle changing protein masks in the next subsection.

2.3.2 Amphipathic and Flexible Masks

In order to address the problem of membrane curvature sensing and generating proteins we will need a mask which is both amphipathic and can have spontaneous curvature. In this subsection we construct such a mask.

To begin, we define the space curve $\psi : \mathbb{R} \to \mathbb{R}^3$, parametrized by arclength, to represent the center line of the protein. At each point along this curve we define a body-fixed reference frame, $(\mathbf{e}_1(s), \mathbf{e}_2(s), \mathbf{e}_3(s))$, according to the following rules:

(i) $\mathbf{e}_3(s) = d\psi/ds$ (note: $\|d\psi/ds\| = 1$ in the arclength parametrization),

(ii) $\mathbf{e}_2(s)$ is in the direction perpendicular to $\mathbf{e}_3$ and towards the lipid bilayer when the protein is associated with it,

(iii) $\mathbf{e}_1 = \mathbf{e}_2 \times \mathbf{e}_3$.

The rotation of this coordinate system along the arclength of the protein is described by the strain vector [55], $\mathbf{\Omega}(s)$,

$$\frac{d\mathbf{e}_i}{ds} = \mathbf{\Omega} \times \mathbf{e}_i. \tag{2.3.3}$$

Note that from the definition of $\mathbf{e}_i$ we also have the relation $\mathbf{e}_i \times \mathbf{e}_j = \epsilon_{ijk}\mathbf{e}_k$, where ϵ_{ijk} is the antisymmetric symbol and repeated indices are implicitly summed over (Einstein summation convention). Therefore, we can also write Equation 2.3.3 as (c.f. equation (2) in [56])

$$\frac{d\mathbf{e}_i}{ds} = -\epsilon_{ijk}\Omega_j\mathbf{e}_k, \tag{2.3.4}$$

where Ω_j are the components of $\mathbf{\Omega}$ in the body-fixed basis, $\Omega_j = \mathbf{e}_j \cdot \mathbf{\Omega}$. Ω_1 and Ω_2 describe the bending (curvature) of the protein, while Ω_3 gives the twist (torsion) of the protein [57]. Given $\mathbf{\Omega}(s)$ for each s, and set of initial conditions $\psi(0)$, $\mathbf{e}_2(0)$, $\mathbf{e}_3(0)$ (we do not need to be given $\mathbf{e}_1(0)$ independently since $\mathbf{e}_1 = \mathbf{e}_2 \times \mathbf{e}_3$), the space curve $\psi(s)$ is completely specified by Equation 2.3.4 and $\psi(s) = \int_0^s \mathbf{e}_3(s')\, ds' + \psi(0)$, which follows from the definition of $\mathbf{e}_3$.

The bending and twisting energy of ψ is determined by $\mathbf{\Omega}$ according to [56, 57]

$$E[\mathbf{\Omega}] = \int_0^L \sum_{i=1}^{3} \frac{k_i}{2} \left(\Omega_i - \overline{\Omega}_i\right)^2 \, ds, \tag{2.3.5}$$

where $\overline{\Omega}_i$ are the spontaneous curvatures and torsion, k_1 and k_2 are the bending moduli, k_3 is the twisting modulus and L is the length of the protein. This term will need to be included in the SCFT free energy functional in order to model balancing the energy costs of deforming the protein with the energy gains of being associated with the membrane. As described in the previous subsection, we will also need a concentration profile (mask) for the protein in order to include it within the SCFT formalism. In what follows we deviate from the notation of subsection 2.3.1 since it is more convenient to denote the two parts of the protein mask by $\phi_{P,\pm}$ rather than ϕ_W and ϕ_V. We associate concentration profiles with ψ according to the following rule:

$$\phi_{P,\pm}(\mathbf{r}) = \int_0^L \theta\left(\pm[\mathbf{r} - \psi(s)] \cdot \mathbf{e}_2(s)\right) \varphi\left(\|\mathbf{r} - \psi(s)\|\right) \, ds, \tag{2.3.6}$$

where $\theta(x) = \begin{cases} 1 & x > 0 \\ 0 & x \leq 0 \end{cases}$ and $\varphi(x) = \tanh(b(a-x)) + 1$, where a is the radius of the protein and $b > 0$ is a parameter for the sharpness of the protein interface. From the definition of $\mathbf{e}_2$, $\phi_{P,+}$ is the protein concentration associated with membrane (hydrophobic), while $\phi_{P,-}$ will interact with the solvent (hydrophilic).

Therefore, the free energy functional which includes the polymer SCFT as well as the protein elasticity is

$$\mathcal{F} = \mathcal{F}_{\text{poly}} + E[\mathbf{\Omega}] + \mathcal{F}_{\text{prot}},$$

where $\mathcal{F}_{\text{poly}}$ is the free energy of the polymers (given by Equation 2.2.4), $E[\mathbf{\Omega}]$ is the bending energy of the protein (given by Equation 2.3.5) and $\mathcal{F}_{\text{prot}}$ is the energy from the polymer-protein interaction given by

$$\begin{aligned}\mathcal{F}_{\text{prot}} = \frac{1}{V}\int d\mathbf{r}\,\{&\chi_{AP,+}N\phi_A\phi_{P,+} + \chi_{BP,+}N\phi_B\phi_{P,+} + \chi_{CP,+}N\phi_C\phi_{P,+} + \\ &\chi_{AP,-}N\phi_A\phi_{P,-} + \chi_{BP,-}N\phi_B\phi_{P,-} + \chi_{CP,-}N\phi_C\phi_{P,-} - \\ &\eta(1-\phi_A-\phi_B-\phi_C-\phi_{P,+}-\phi_{P,-})\}\,.\end{aligned}$$

Functional differentiation of this free energy with respect to the polymer fields ($\{\omega_\alpha, \phi_\alpha, \eta\}$) gives the SCFT equations for a fixed protein, while differentiation with respect to the protein variables (the curvatures, initial position and initial direction) gives a "force" acting on the protein for the current polymer configurations. Hence, finding the solution of this system requires first solving the SCFT equations to find the best polymer configurations for the present protein configuration, then changing the protein a small amount in the direction of the polymer "force" acting on it and repeating this process until the protein is in equilibrium with the polymers. Details regarding the numerical implementation of finding polymer fields which solve the SCFT equations are given in chapter 3.

Chapter 3

Numerical Implimentation

3.1 Solving SCFT Equations By Iteration With Anderson Mixing

As we have seen in section 2.2, the chemical potential fields, ω_α, concentration fields, ϕ_α, and pressure field, η, which are solutions to the SCFT equations are related to one another. Therefore, if we define a function, $G(\{\omega_\alpha, \eta\})$, according to Algorithm 2.2.1 (i.e. G is the mapping $\{\omega_\alpha, \eta\} \mapsto \{\omega'_\alpha, \eta'\}$), then SCFT solutions would also solve

$$\{\omega_\alpha, \eta\} = G(\{\omega_\alpha, \eta\}), \tag{3.1.1}$$

i.e. $\{\omega_\alpha, \eta\}$ is a fixed point of the function G.

Given the equivalence of solving the SCFT equations to solving a fixed point problem established above, we will now consider the following general fixed point problem. Let X be a Real Hilbert Space, with inner product denoted by $\langle \cdot, \cdot \rangle$ and let $G : X \to X$ be a function on that space. We wish to find $x \in X$ such that $x = G(x)$.

A simple tactic for solving such problems is by iteration: begin with some initial point x_0 and define a sequence recursively according to $x_{n+1} = G(x_n)$. One might hope that $\lim_{n\to\infty} x_n$ would converge and be equal to a fixed point. In fact, this is true for a certain class of functions, as the following theorem shows [58]:

Theorem 1 (Banach Fixed Point Theorem)**.** *Let $U \subseteq X$ be a closed subset under the mapping G. Suppose that for all $x, y \in U$*

$$\|G(x) - G(y)\| \leq \epsilon \|x - y\|, \tag{3.1.2}$$

where $\epsilon \in [0, 1)$ and $\|\cdot\|$ is the norm induced by the inner product on X, i.e. $\|x\|^2 = \langle x,\ x\rangle$. Then G has a unique fixed point, x^*, in U and given any $x_0 \in U$, the sequence $x_0, G(x_0), G(G(x_0)) \ldots$ converges to x^*.

A function satisfying Equation 3.1.2 is called a contraction mapping on U and U is call the basin of attraction for the fixed point x^*. Note that the fixed point is only unique when considering points in U; G may have other fixed points in X which lie outside that subset.

It is possible that the subset U is quite small compared to X or perhaps even that G is not a contraction mapping at all. In this case we can attempt to construct a contraction mapping with a larger basin of attraction in the following way. Define a new function

$$G_\lambda(x) = (1 - \lambda)x + \lambda G(x), \tag{3.1.3}$$

where $\lambda \in [0, 1]$ is called the mixing parameter. Notice that if x^* is a fixed point of G then it is also a fixed point of G_λ. Also note that if $\lambda = 0$ then G_λ

is the identity function and if $\lambda = 1$ then $G_\lambda = G$. Therefore, in some sense, G_λ is "less harsh" than G in terms of how much x is altered. In the SCFT literature, solving the SCFT equations by iterating the function G_λ rather than G is called "simple mixing."

If one chooses the correct value of λ, the convergence of x_n to the fixed point can be greatly improved. However, the choice of λ is problem-dependant since if λ is too small then the convergence can be made very slow, but if it is too large then G_λ may not have a basin of attraction which includes the initial condition the user has chosen. All of these considerations depend on the details of G (which in turn depend on the details of the system begin studied) and x_0. Therefore, in practice, λ is chosen essentially arbitrarily by trial and error.

The method of Anderson mixing is another modification of solving fixed point problems using iteration. The idea behind this method is to use more than just the current x_n in determining the next iteration, i.e. the algorithm includes some memory of past iterations. Anderson mixing is named after Donald G. Anderson, who proposed the method in the context of solving non-linear integral equations iteratively [59]. The method has since found use in other areas of physics and chemistry (see e.g. [60, 61]). Here we use a generalization of the derivation presented by Ng [60]. Suppose we have a sequence of m points, $x_0, x_1, x_2, \ldots, x_{m-1}$ and we wish to combine them in some optimal way in order to come closer to a fixed point of G. The simplest idea would be to choose a linear combination of the previous points:

$$x_m = x_{m-1} + \sum_{n=0}^{m-2} c_n (x_n - x_{m-1}). \tag{3.1.4}$$

Note that there are only $m-1$ free constants since we also demand that the sum of the coefficients in the linear combination be equal to unity, i.e. $\sum_{n=0}^{m-1} c_n = 1 \implies c_{m-1} = 1 - \sum_{n=0}^{m-2} c_n$. We wish to choose the constants c_n in order to minimize $\|G(x_m) - x_m\|$ since this will make x_m as close to being a fixed point as possible. In order to derive a simple analytic expression we make the further simplifying assumption that G is a linear function. Using that assumption and the definition $d_n = G(x_n) - x_n$, we can write

$$\begin{aligned}\|G(x_m) - x_m\|^2 &= \left\| d_{m-1} + \sum_{n=0}^{m-2} c_n d_n \right\|^2 \\ &= \|d_{m-1}\|^2 + 2\sum_{n=0}^{m-2} c_n \langle d_{m-1},\ d_n - d_{m-1}\rangle + \\ &\qquad \sum_{n=0}^{m-2}\sum_{k=0}^{m-1} c_n c_k \langle d_n - d_{m-1},\ d_k - d_{m-1}\rangle \,. \end{aligned} \tag{3.1.5}$$

By differentiating Equation 3.1.5 we find that the solution to the optimization problem is given by the solution to the linear system

$$\mathbf{b} = A\mathbf{c}, \tag{3.1.6}$$

where $\mathbf{b}$ is the vector with elements $b_n = \langle d_{m-1},\ d_{m-1} - d_n\rangle$, A is the matrix with elements $A_{nk} = \langle d_{m-1} - d_n,\ d_{m-1} - d_k\rangle$, and $\mathbf{c}$ is the vector with elements given by the coefficients of the linear combination, c_n.

The final result returned by Anderson mixing is not x_m as defined in Equation 3.1.4, but rather

$$x_m = G(x_{m-1}) + \sum_{n=0}^{m-2} c_n \left[G(x_n) - G(x_{m-1})\right], \tag{3.1.7}$$

where the c_n's are the solution to Equation 3.1.6. This ensures that if G is a non-linear function that future iterates are not limited to the subspace spanned

by the previous ones. Of course, if G is non-linear then the c_n's used in the linear combination are only an approximation to the true optimal coefficients, however we assume that x_m will still at least be closer to the fixed point than the previous iterations, even if it is not as close as it could possibly be.

Thus, the full Anderson mixing algorithm is as follows:

Algorithm 3.1.1. Input: tol, maxit, m, x_0

1. Initialize: $y_0 = G(x_0)$; $d_0 = y_0 - x_0$; $x_1 = y_0$; $n = 0$
2. while $n \leq m$: //build up memory from initial condition
3. $n = n + 1$; $y_n = G(x_n)$; $d_n = y_n - x_n$
4. if $\|d_n\| <$ tol then return y_n
5. Construct $(n-1)$-component vector $\mathbf{b}$ such that $b_k = \langle d_n,\ d_n - d_{n-k} \rangle$, $k = 1, 2, \ldots, n-1$.
6. Construct $(n-1)\times(n-1)$ matrix A such that $A_{ij} = \langle d_n - d_{n-i},\ d_n - d_{n-j} \rangle$
7. Solve $A\mathbf{c} = \mathbf{b}$
8. $x_{n+1} = G(x_n) + \sum_{k=1}^{n-1} c_k \left[G(x_{n-k}) - G(x_n) \right]$
9. while $n <$ maxit: //continue algorithm with present memory size
10. $n = n + 1$; $y_n = G(x_n)$; $d_n = y_n - x_n$
11. if $\|d_n\| <$ tol then return y_n
12. Construct $(m-1)$-component vector $\mathbf{b}$ such that $b_k = \langle d_n,\ d_n - d_{n-k} \rangle$, $k = 1, 2, \ldots, m-1$.

13. `Construct` $(m-1)\times(m-1)$ `matrix` A `such that` $A_{ij} = \langle d_n - d_{n-i},\ d_n - d_{n-j} \rangle$

14. `Solve` $A\mathbf{c} = \mathbf{b}$

15. $x_{n+1} = G(x_n) + \sum_{k=1}^{m-1} c_k \left[G(x_{n-k}) - G(x_n) \right]$

Where `tol`, `maxit`, and m are input parameters from the user giving the convergence tolerance, maximum number of iterations and memory size, respectively.

In the actual implementation of the code for this thesis, we have combined Anderson mixing with simple mixing by also choosing a mixing parameter λ and using G_λ as the function in the Anderson mixing algorithm instead of simply G itself. For cases where no protein mask is present (e.g. computing the bilayer mechanical properties), only Anderson mixing was required so $\lambda = 1$ was used. However, with a protein mask it seemed that G alone was not a contraction mapping and $\lambda = 0.25$ was used instead in order for the system to converge. The inner product used for these systems is the natural one for a multi-component function space:

$$\langle \{\omega_\alpha, \eta\},\ \{\omega'_\alpha, \eta'\} \rangle = \sum_\alpha \left(\int d\mathbf{r}\ \omega_\alpha(\mathbf{r}) \omega'_\alpha(\mathbf{r}) \right) + \int d\mathbf{r}\ \eta(\mathbf{r}) \eta'(\mathbf{r}). \qquad (3.1.8)$$

3.2 Single Transmembrane Protein in a Bilayer

The main system which we consider in this thesis is one in which there is a single, cylindrical inclusion which spans the entire width of the membrane and in fact is much larger than the membrane thickness (however this is not

a significant limitation, see subsection 1.1.3). In this section we specialize the SCFT equations given in section 2.2 to this system.

3.2.1 SCFT Equations in 2D Cylindrical Coordinates

This system is rotationally symmetric, hence it lends itself well to cylindrical coordinates in which we do not explicitly include the angular variable. In this coordinate system we have

$$\nabla^2 \mapsto \frac{1}{r}\frac{\partial}{\partial r}\left(r\frac{\partial}{\partial r}\right) + \frac{\partial^2}{\partial z^2}$$
$$\int d\mathbf{r} \mapsto 2\pi \int r dr dz.$$

Hence, the equations for the propagators for this system are

$$\mathcal{Q}_1\left[\{\omega_\alpha\}\right] = \frac{2\pi}{V}\int dr dz\; r q_A^\dagger(r,z,N_A) = \frac{2\pi}{V}\int dr dz\; r q_B^\dagger(r,z,N_B) \tag{3.2.1}$$

$$\mathcal{Q}_2\left[\omega_C\right] = \frac{2\pi}{V}\int dr dz\; r q_C(r,z,N_C) \tag{3.2.2}$$

$$\frac{\partial q_\alpha}{\partial s} = \sigma_\alpha^2\left(\frac{\partial^2 q_\alpha}{\partial r^2} + \frac{1}{r}\frac{\partial q_\alpha}{\partial r} + \frac{\partial^2 q_\alpha}{\partial z^2}\right) - \omega_\alpha q_\alpha,\ \alpha \in \{A,B,C\}, \tag{3.2.3}$$

while the other SCFT equations remain essentially unchanged.

3.2.2 Alternating Direction Implicit (ADI) Method

Equation 3.2.3 needs to be solved numerically when implementing SCFT. The Alternating Direction Implicit (ADI) Method is a finite differencing, operator splitting method used for solving partial differential equations. The method works well for equations with one time and two space variables, as

in Equation 3.2.3 (indeed, it was first developed by Peacemand and Rachford [62] to solve diffusion equations related to heat flow in two dimensions).

Since this is a finite difference method, we consider a discrete lattice of spatial/contour (playing the role of time in our equation), $\{r_i, z_j, s_k\}$, where $1 \leq i \leq N_r$, $1 \leq j \leq N_z$, $1 \leq k \leq N_s$ (in the implementation used in the thesis $N_r = N_z = 150$, while N_s varied in order to obtain the desired accuracy of the propagators). The spacing of the lattice will be given by $\Delta r = r_i - r_{i-1}$, $\Delta z = z_j - z_{j-1}$ and $\Delta s = s_k - s_{k-1}$. For simplicity we will denote $q(r_i, z_j, s_k)$ by $q^k_{i,j}$ and $\omega(r_i, z_j)$ by $\omega_{i,j}$. On this lattice Equation 3.2.3 is approximated by a difference equation. The ADI method uses centred difference approximations for the spatial variables:

$$\frac{\partial^2 q(r,z,s)}{\partial r^2} \mapsto \delta_r^2 q^k_{i,j} = \frac{1}{(\Delta r)^2}\left(q^k_{i+1,j} - 2q^k_{i,j} + q^k_{i-1,j}\right) \tag{3.2.4}$$

$$\frac{\partial q(r,z,s)}{\partial r} \mapsto \delta_r q^k_{i,j} = \frac{1}{2\Delta r}\left(q^k_{i+1,j} - q^k_{i-1,j}\right) \tag{3.2.5}$$

$$\frac{\partial^2 q(r,z,s)}{\partial z^2} \mapsto \delta_z^2 q^k_{i,j} = \frac{1}{(\Delta z)^2}(q^k_{i,j+1} - 2q^k_{i,j} + q^k_{i,j-1}), \tag{3.2.6}$$

and a forward (half-step) difference approximation in the contour variable

$$\frac{\partial q(r,z,s)}{\partial s} \mapsto \delta_s q^k_{i,j} = \frac{1}{\Delta s/2}\left(q^{k+1/2}_{i,j} - q^k_{i,j}\right). \tag{3.2.7}$$

The details of the ADI method are given in Appendix B. Here we conceptually lay out the method. Each step takes a full spatial solution forward in the contour variable, $q^k_{i,j} \to q^{k+1}_{i,j}$, by taking two half steps, $q^k_{i,j} \to q^{k+1/2}_{i,j} \to q^{k+1}_{i,j}$. In the first half step, we keep the z part of the differential operator at k, while advancing the r part of the differential operator to $k + 1/2$

$$\delta_s q^k_{i,j} = \sigma^2 \delta_r^2 q^{k+1/2}_{i,j} + \frac{\sigma^2}{r_i}\delta_r q^{k+1/2}_{i,j} + \sigma^2 \delta_z^2 q^k_{i,j} - \omega_{i,j}\left(\frac{q^{k+1/2}_{i,j} + q^k_{i,j}}{2}\right).$$

After some rearrangement, one can write a linear system of equations for $q_{i,j}^{k+1/2}$ in terms of $q_{i,j}^{k}$ which can be represented using a tridiagonal matrix. This is convenient since such systems can be quickly and efficiently solved by using the tridiagonal matrix algorithm (TDMA), also known as the Thomas algorithm [63, 64]. In the second half step we keep the r part of the differential operator at $k + 1/2$ and advance the z part to $k + 1$

$$\delta_s q_{i,j}^{k+1/2} = \sigma^2 \delta_r^2 q_{i,j}^{k+1/2} + \frac{\sigma^2}{r_i} \delta_r q_{i,j}^{k+1/2} + \sigma^2 \delta_z^2 q_{i,j}^{k+1} - \omega_{i,j} \left(\frac{q_{i,j}^{k+1} + q_{i,j}^{k+1/2}}{2} \right).$$

Again, we can rearrange this into a tridiagonal system of linear equations and apply the TDMA in order to obtain a full spatial solution at $k + 1$. This process is repeated to take the initial condition at $k = 1$ through all the subsequent values of k, hence obtaining a complete solution to the PDE.

3.3 A Single Surface Protein on a Bilayer

During this thesis work was also done on a system in which the protein was embedded on the surface of the membrane rather than spanning the entire thickness. This configuration of the protein breaks the rotational symmetry used in the previous section to reduce the problem to two dimensions. Therefore, in this case SCFT needs to implemented differently, as detailed in the following subsections.

3.3.1 SCFT Equations in 3D Cartesian Coordinates

Since this system has no canonical symmetry to take advantage of, we use ordinary Cartesian coordinates as these are the simplest real-space coordinates. In this coordinate system we have

$$\nabla^2 \mapsto \frac{\partial^2}{\partial x^2} + \frac{\partial^2}{\partial y^2} + \frac{\partial^2}{\partial z^2}$$
$$\int d\mathbf{r} \mapsto \int dxdydz.$$

Hence, the equations for the propagators for this system are

$$\mathcal{Q}_1\left[\{\omega_\alpha\}\right] = \frac{1}{V}\int dxdydz\ q_A^\dagger(x,y,z,N_A) = \frac{1}{V}\int dxdydz\ q_B^\dagger(x,y,z,N_B) \tag{3.3.1}$$

$$\mathcal{Q}_2\left[\omega_C\right] = \frac{1}{V}\int dxdydz\ q_C(x,y,z,N_C) \tag{3.3.2}$$

$$\frac{\partial q_\alpha}{\partial s} = \sigma_\alpha^2\left(\frac{\partial^2 q_\alpha}{\partial x^2} + \frac{\partial^2 q_\alpha}{\partial y^2} + \frac{\partial^2 q_\alpha}{\partial z^2}\right) - \omega_\alpha q_\alpha,\ \alpha \in \{A,B,C\}, \tag{3.3.3}$$

while, again, the other SCFT equations remain essentially unchanged.

3.3.2 Pseudospectral Method

Once again Equation 3.3.3 needs to be solved numerically. However, now with three spatial dimensions and one time dimension, the ADI method is no longer sufficiently fast or accurate. Instead, we apply a method which takes advantage of the form of the differential equation we aim to solve.

Abstractly, we can think of Equation 3.3.3 as $\partial_s q = \mathcal{L}q$, where $\mathcal{L}$ is the differential operator $\sigma^2\nabla^2 - \omega/2 - \omega/2$ (the reason for splitting the ω term into two parts will be made clear below) and the subscript α's have been dropped

for brevity. In this form, theory of first order differential equations tells us that

$$q(\mathbf{r}, s + \Delta s) = e^{\Delta s \mathcal{L}} q(\mathbf{r}, s).$$

The operator $e^{\Delta s \mathcal{L}}$ can be factored into three parts by using each of the three terms in $\mathcal{L}$ [65]

$$e^{\Delta s \mathcal{L}} = e^{-\Delta s \omega/2} e^{\Delta s \sigma^2 \nabla^2} e^{-\Delta s \omega/2} + \mathcal{O}(\Delta s^3)$$

(the reason for splitting ω into two parts was to allow the factorization to be correct up to order Δs^3). The first and final parts of the operator are trivially applied to the real-space representation of q, while the second part is easily applied in Fourier space. Hence, if $\mathcal{F}$ is the Fourier transform operation then we can write

$$q(\mathbf{r}, s + \Delta s) = e^{-\Delta s \omega/2} \mathcal{F}^{-1} \left[e^{\Delta s \sigma^2 k^2} \mathcal{F} \left[e^{-\Delta s \omega/2} q(\mathbf{r}, s) \right] \right]. \tag{3.3.4}$$

In the code for this thesis we use the fast Fourier transform (FFT) to perform the Fourier transforms, allowing for a very efficient numerical implementation. Moreover, since the derivative operations are done in Fourier space rather than by finite differences we can use a much less dense spatial grid while keeping good numerical accuracy. This is important since storing many points on a three-dimensional grid can quickly become very memory and time intensive. In this work a $32 \times 32 \times 32$ grid was used (compared with the 150×150 grid used in the 2D case).

3.3.3 Challenges of Complicated Masks

The reason for considering surface bound proteins was to answer questions regarding membrane curvature sensing and generating proteins. This requires a protein with some spontaneous curvature and hence the mask which represents the protein in SCFT is no longer simply cylindrical (see subsection 2.3.2 for details regarding these masks). These complicated masks effectively serve as a boundary condition for this system and hence finding solutions becomes significantly more difficult. Even with the Anderson mixing iterative scheme described in section 3.1 and the accurate pseudospectral differential equation solution method described in subsection 3.3.2, convergence was never achieved for a system involving a curved surface protein.

To attempt to circumvent this problem we tried other schemes for solving the SCFT equations including conjugate gradient methods, direct heuristic optimization of the free energy functional, and Newton's method-type algorithms (with automatic differentiation [66] for computational efficiency). However, none of these were ever able to out-perform the Anderson mixing scheme and none could find a solution for the curved protein system. For this reason, despite much time and effort spent on this project, no results will be presented regarding curvature sensing or generating proteins. However, these problems only concern the numerical implementation of the theory developed here, which we believe to be valuable nonetheless. This theoretical framework may be used in a future work with a more robust numerical implementation.

Chapter 4

Results for a Transmembrane Protein in a Bilayer

In this chapter we present the results obtained for the system composed of a bilayer membrane with a long, cylindrical, hydrophobic insertion spanning the entire membrane width. This system provides a simple model of transmembrane proteins, as well as the opportunity to study an interesting variation on wetting phase transitions.

Throughout this chapter we will be considering three different values of the Flory-Huggins parameters which describe the bilayer, $\chi_{AB}N = \chi_{BC}N = 15, 20, 25$. These values correspond to soft, medium and hard bilayers (in the sense of their bending rigidities), respectively. In addition, we consider three different values of the radius of the cylindrical insertion, $R = 0.1, 2, 20$ (in units of the polymer radius of gyration). These values correspond to distances which are much shorter, approximately equal to, and much greater than the thickness of the membrane.

4.1 Wetting Transition

We begin with the results regarding the wetting phase transition. During this study we began with the membrane against a non-interacting insertion, i.e. $\chi_{AW}N = \chi_{CW}N = 0$. Since the inclusion is normally inserted with respect to the bilayer, this configuration corresponds to a wetting angle of $\theta_e = 90°$. The strength of the protein-membrane interaction was then increased one unit at a time, i.e. $\chi_{AW}N = \chi_{CW}N = 1, 2, 3, \ldots$, with the previous SCFT solution used as the initial condition for the next computation. As $\chi_{AW}N$ increases, the bilayer covers more of the insertion surface and θ_e decreases. At each value of $\chi_{AW}N$, the membrane hydrophobic interfaces (defined to be where $\phi_A = \phi_B$ in the SCFT solution) were found. We then define complete wetting in terms of these interfaces, viz. complete wetting has occurred once the interfaces no longer intersect the hydrophobic insertion. Some representative plots of the bilayer in the various configurations described here are shown in Figure 4.1.

Examining Figure 4.1, we see that the concentration of lipids (AB-diblocks) at the insertion surface increases continuously until a full-fledged monolayer is formed. Therefore, we conclude that this is a second order Cahn-like wetting phase transition, similar to that found previously in another polymer system [49]. This result is the same for each different set of membrane parameters and protein radii (not all shown). However, those parameters do determine when the transition occurs. This can be seen in Figure 4.2, in which θ_e is plotted against $\chi_{AW}N$. We see that the trend is softer bilayers and larger protein radii tend to decrease the value of $\chi_{AW}N$ at which the transition takes place. This result makes sense since, as mentioned in subsection 1.3.2, the primary energy

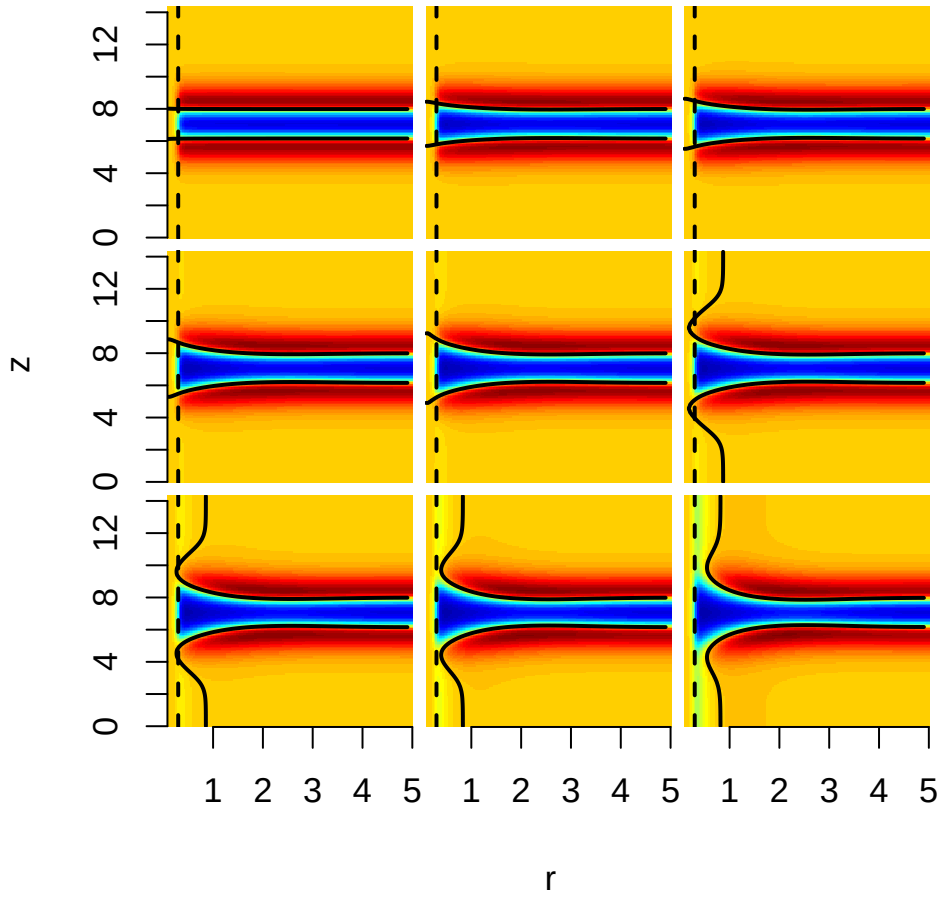

Figure 4.1: Plotted is $\phi_A - \phi_B$ as a function of r and z. The solid black lines show the bilayer hydrophobic interface, $\phi_A = \phi_B$, and the dashed black line shows the protein insertion surface, $\phi_W = 0.5$. The value of $\chi_{AW}N$ increases from left to right and top to bottom as follows: 0, 30, 40, 50, 60, 65, 70, 80, 90. We would say that complete wetting is achieved between $\chi_{AW}N = 70$ and 80 since the solid and dashed lines no longer intersect after that point.

barrier to wetting is the formation of the kink which is necessary to connect the wetting monolayer with the bilayer membrane. This energy barrier will be lower for membranes which have smaller bending rigidities and for larger protein radii (since the radius of curvature of the kink will be larger), hence wetting would occur at lower values of $\chi_{AW}N$. Note that in Figure 4.2 the wetting angle does not suddenly drop to zero where the lines end in the plot (which would indicate a first order phase transition); the wetting angle simply because more difficult to numerically determine accurately after those points. However, since this difficulty arises in the same way for all parameter values, where the lines end is a proxy for where the phase transition occurs.

4.2 Consistency of Elastic Theory with SCFT

Next, we will use the membrane hydrophobic interface data obtained in the calculations described in the previous section (the solid black lines in Figure 4.1) in order to compare SCFT with elastic theory. By taking the distance between the top and bottom curves which describe the interfaces, we can determine the thickness of the bilayer as a function of the radial coordinate. This is the same quantity which can be predicted using the elastic theory of Tjörnhammar and Edholm [40] discussed in subsection 1.2.2. Recall that the mechanical properties of the bilayer are parameters of this theory and that they can be calculated directly within SCFT. Using the methods described in subsection 2.2.3, we determine the stretching modulus, k_s, the surface tension, γ, and the bending modulus, k_b. Additionally, from the thickness profile obtained in SCFT, we determine the natural thickness, t_0 and the boundary

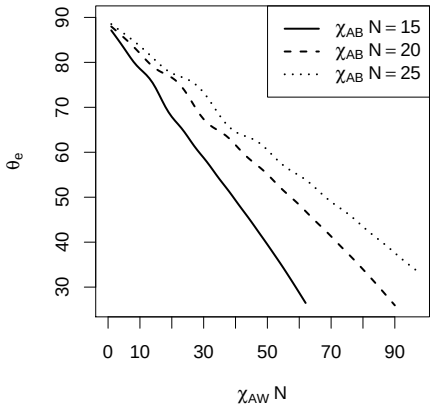

(a) $R = 0.1$

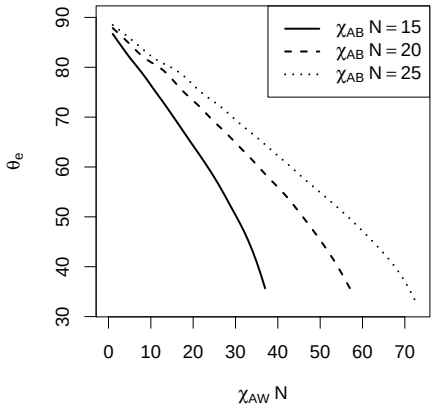

(b) $R = 2$

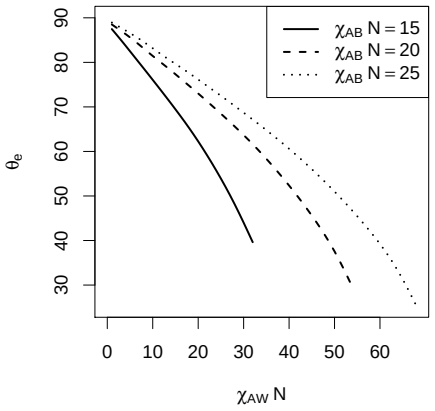

(c) $R = 20$

Figure 4.2: Plots showing the wetting angle of the bilayer as a function of $\chi_{AW}N$. Solid, dashed and dotted lines correspond to $\chi_{AB}N = 15, 20, 25$ (i.e. soft, medium and rigid bilayers), respectively. Panels (a), (b), and (c) show the data for the protein radius being equal to $0.1, 2, 20$ (i.e. much smaller than, approximately equal to and much greater than bilayer thickness), respectively. The small oscillations which appear are due to numerical imperfections when determining the wetting angle.

conditions, $t(R)$ and $t'(R)$, where R is the protein radius. We can then use all this information obtained from the SCFT calculation to solve Equation 1.2.2 numerically. In order to determine if the elastic theory is consistent with SCFT we then compare this solution to the SCFT thickness profile.

Figure 4.3 shows some representative thickness profiles obtained from SCFT and elastic theories. The average difference between the two curves is plotted as a function of $\chi_{AW}N$ for the various membrane parameters and protein radii in Figure 4.4. We see that the two theories agree very well (all average deviations $< 8\%$, with the most significant differences occurring near the wetting transition). Therefore it can be concluded that SCFT is consistent with elastic theory in the sense that the profile predictions from elastic theory obtained using the SCFT mechanical properties agree with the SCFT profile predictions.

4.3 Systematics of Profile Boundary Conditions

Given that the predictions of elastic theory are the same as those from the more complicated and more computationally intensive SCFT, it would be desirable if elastic theory could be used in future studies. However, boundary conditions are still required in order to solve the differential equation associated with elastic theory and these cannot be obtained without some additional assumptions. For example, it has been assumed previously [40] that perfect hydrophobic matching occurs (i.e. the membrane thickness changes to perfectly correspond with the protein thickness) and that the membrane is locally flat

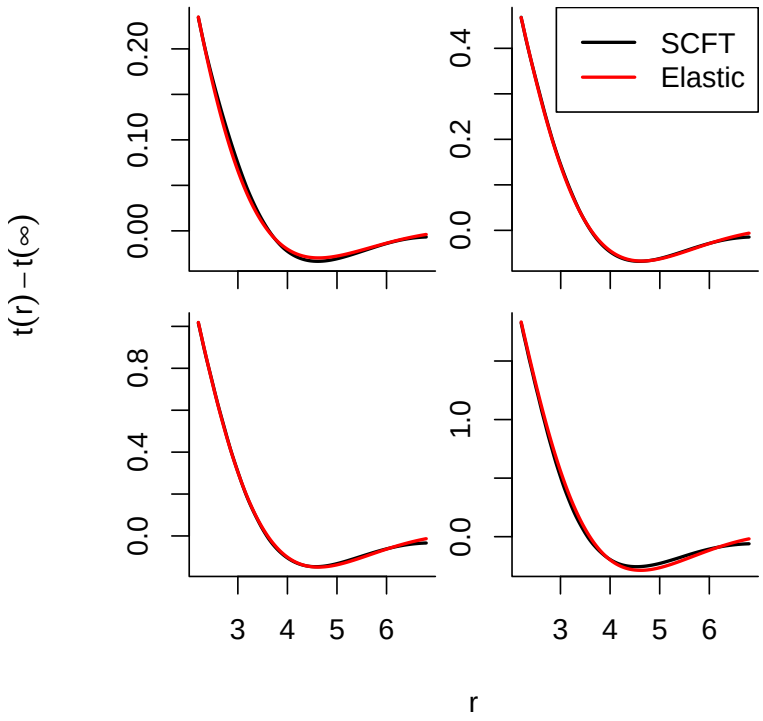

Figure 4.3: Representative plots showing the hydrophobic thickness of the bilayer as a function of r. The black lines show the thickness profile obtained directly from the SCFT calculations, while the red lines are the profiles predicted by elastic theory using the parameters calculated from within SCFT. The equilibrium thickness (thickness when no protein is present) has been subtracted from the values so that a value of zero corresponds to the preferred thickness of the membrane. The value of $\chi_{AW}N$ increases from top to bottom and left to right: $\chi_{AW}N = 10, 20, 40, 60$.

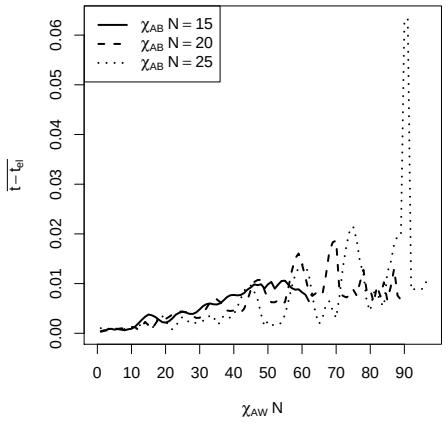

(a) $R = 0.1$

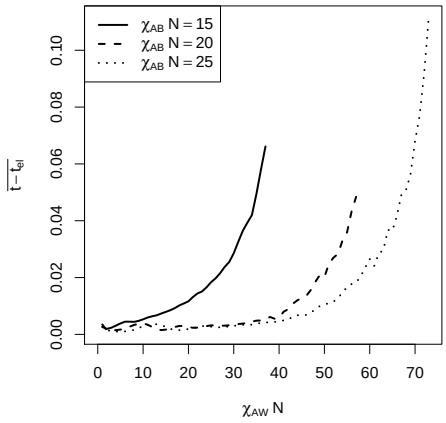

(b) $R = 2$

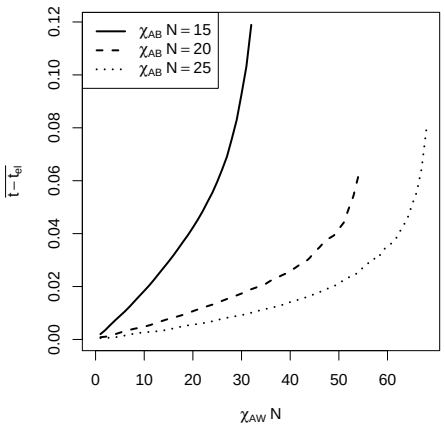

(c) $R = 20$

Figure 4.4: Plots showing the average absolute difference between the SCFT and elastic theory predictions of the hydrophobic thickness of the bilayer, a function of $\chi_{AW}N$. Solid, dashed and dotted lines correspond to $\chi_{AB}N = 15, 20, 25$ (i.e. soft, medium and rigid bilayers), respectively. Panels (a), (b), and (c) show the data for the protein radius being equal to $0.1, 2, 20$ (i.e. much smaller than, approximately equal to and much greater than bilayer thickness), respectively.

near the protein (i.e. the first derivative of the thickness profile is zero at the boundary).

In contrast, SCFT does provide boundary conditions for the profile without additional assumptions. We take advantage of this fact in order to provide systematics of the boundary conditions over the various parameter values used in this study. We hope that the trends revealed here will inform future assumptions used when determining the boundary conditions for elastic theories.

The thickness of the membrane is plotted as a function of $\chi_{AW}N$ in Figure 4.5 for the different membrane parameters and protein radii. Note that for these calculations the hydrophobic mismatch is technically infinite since the protein is much longer than the membrane thickness, however, below the wetting transition, the stretching of the membrane is finite. This plot thus gives an upper bound for the membrane stretching which can occur for different interaction strengths. Perfect hydrophobic matching will occur only if the hydrophobic part of the protein is shorter than the values given in Figure 4.5, otherwise only some membrane stretching will occur. This is an important result since it challenges the assumption given above. The general systematic trend in this data is that the upper bound of membrane stretching increases with the interaction strength and the rate of this increase is a decreasing function of the membrane stretching/bending rigidities. The rate is also an increasing function of the protein radius. Again, these trends are sensible since, as mentioned previously, more rigid bilayers and smaller proteins should result in a system which is more resistant to wetting.

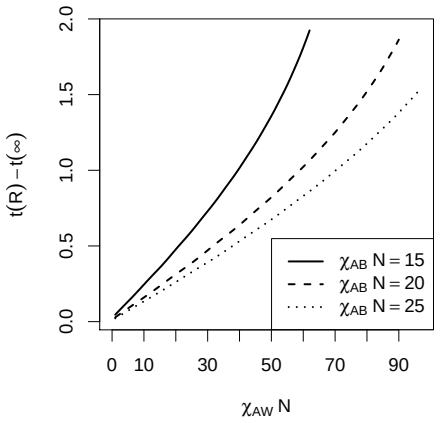

(a) $R = 0.1$

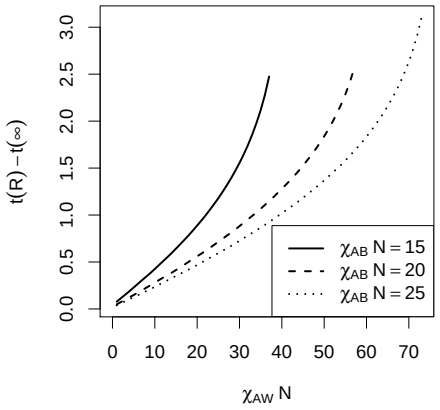

(b) $R = 2$

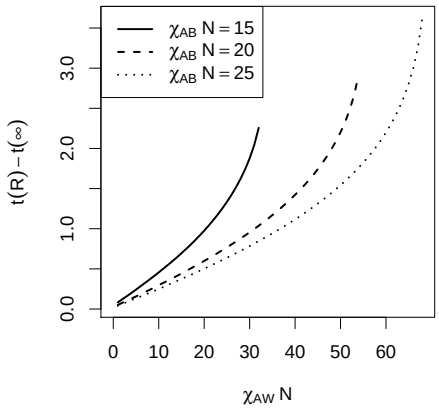

(c) $R = 20$

Figure 4.5: Plots showing the hydrophobic thickness of the bilayer at the protein interface as a function of $\chi_{AW}N$. The equilibrium thickness (thickness when no protein is present) has been subtracted from the values so that a value of zero corresponds to the preferred thickness of the membrane. Solid, dashed and dotted lines correspond to $\chi_{AB}N = 15, 20, 25$ (i.e. soft, medium and rigid bilayers), respectively. Panels (a), (b), and (c) show the data for the protein radius being equal to $0.1, 2, 20$ (i.e. much smaller than, approximately equal to and much greater than bilayer thickness), respectively.

These qualitative trends can be made a little more precise. If the $\chi_{AW}N$ axes of all the plots in Figure 4.5 are scaled by a factor χ_0, given by

$$\chi_0 = 2\chi_{AB}N\left(1 + \frac{1}{\pi R}\right), \tag{4.3.1}$$

then all nine curves approximately collapse onto a single curve, as shown in Figure 4.6. The collapse is not perfect and appears to be worse at higher values of $\chi_{AW}N/\chi_0$. However, Equation 4.3.1 was found using a computationally assisted search and may only be approximate itself. It is possible that it represents the first two terms in an expansion for the true scale factor which relates all nine curves. Future work will be dedicated to developing a physical model which can justify a formula like the one in Equation 4.3.1. Note that this scaling does not apply to the derivative of the thickness profile at the boundary since the trend is non-monotonic in R.

The first derivative of the membrane thickness profile evaluated at the protein surface is plotted as a function of $\chi_{AW}N$ in Figure 4.7 for the different membrane parameters and protein radii. Once again, we see that the previous assumption does not appear to be correct as the slopes are all non-zero. We also again see the same systematic trend as we have seen previously in which softer bilayers are more prone to wetting and hence have steeper initial slopes. Interestingly, however, the trend in terms of protein radius seems to be non-monotonic, with the mid-sized protein resulting in the shallowest initial slopes.

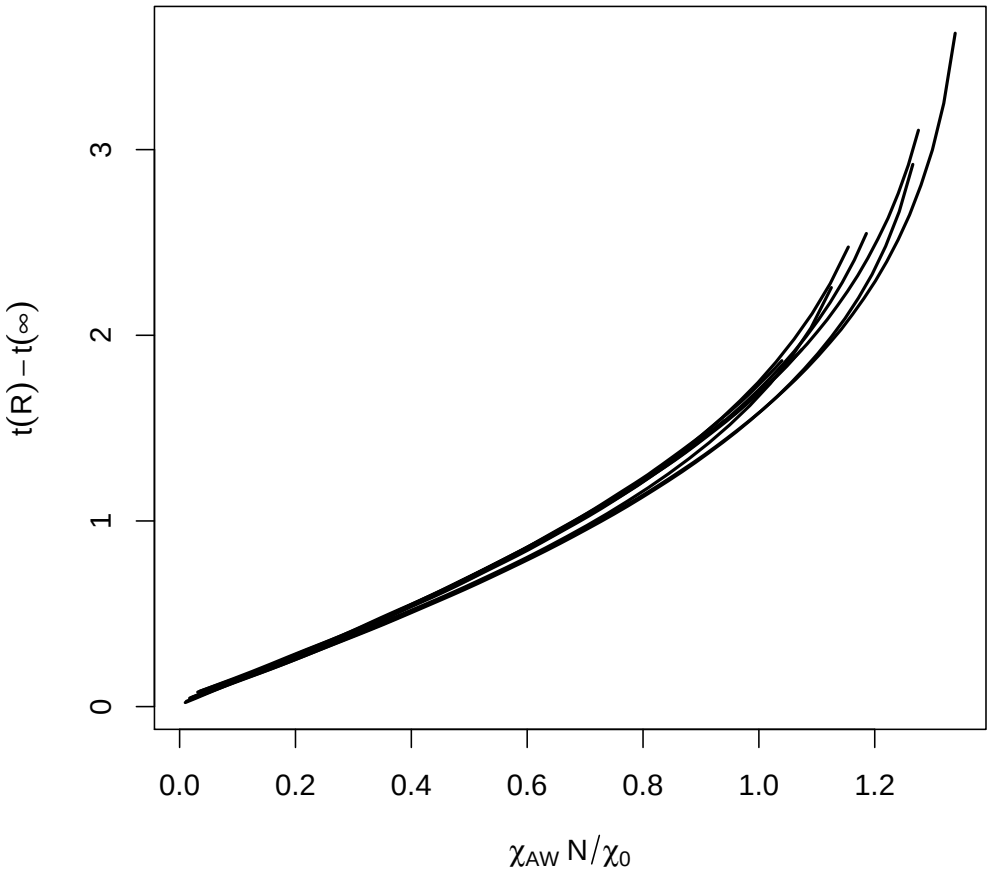

Figure 4.6: Same curves as in Figure 4.5 with the $\chi_{AW}N$ axes scaled by χ_0, defined in Equation 4.3.1. All nine curves approximately collapse onto a single curve.

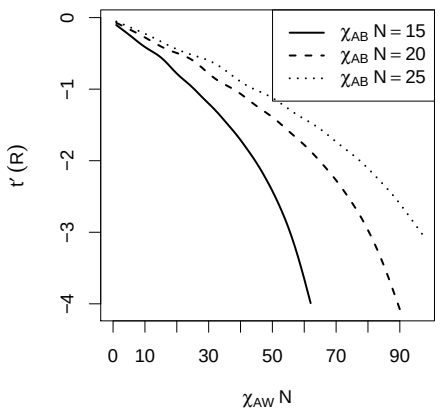

(a) $R = 0.1$

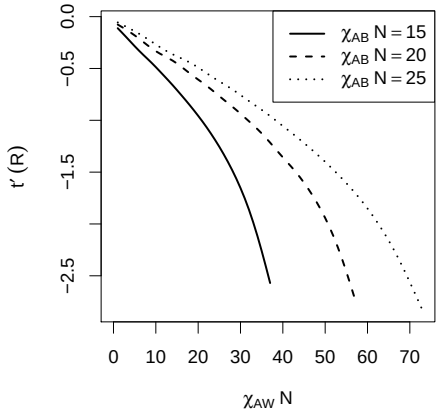

(b) $R = 2$

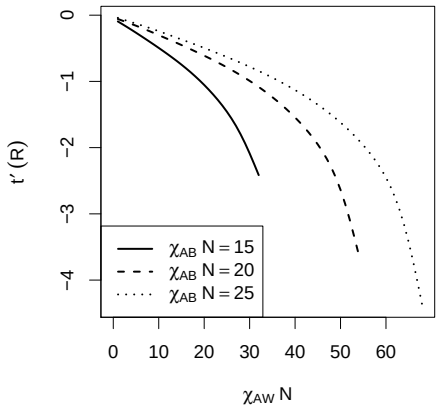

(c) $R = 20$

Figure 4.7: Plots showing the first derivative of the hydrophobic thickness of the bilayer at the protein interface as a function of $\chi_{AW}N$. Solid, dashed and dotted lines correspond to $\chi_{AB}N = 15, 20, 25$ (i.e. soft, medium and rigid bilayers), respectively. Panels (a), (b), and (c) show the data for the protein radius being equal to $0.1, 2, 20$ (i.e. much smaller than, approximately equal to and much greater than bilayer thickness), respectively. The small oscillations which appear are due to numerical imperfections when determining the slope of the thickness profile.

Chapter 5

Towards an Analytical Framework for Computing Mechanical Properties of Membranes Within SCFT

5.1 Framework Motivation and Derivation

The process for determining the mechanical constants of membranes described in subsection 2.2.3 is time consuming ($\sim$ 2 days worth of computation) because it requires solving the SCFT equations many times in order to explicitly determine how the free energy changes as the membrane is deformed. However, it should, in principle, be possible to determine the mechanical constants of a membrane from the SCFT field solutions themselves, rather than using the free energy. This idea as been applied to other systems in order to develop analytical expressions for the surface tension and bending moduli of interfaces (see e.g. [67, 68]). In this section we work towards similar expressions for the SCFT of lipid bilayers. To do this we will apply perturbation theory to a general constrained optimization problem.

We begin with some free energy functional, $F[\phi]$, which depends on a set of fields here simply represented by ϕ for brevity. This functional could, for example, be the one given in Equation 2.2.4, however we need not specify it yet. Next, we imagine there are some constraints, $\{G_i[\phi; h] = 0\}_{i=1}^{n}$, which play the roll of specifying the shape of a membrane. Note that each G_i is not a functional since its result is a new function, not a scalar. The idea is that each G_i can be thought of as including many constrains, one at each point on the membrane. The constraint depends on the fields involved in the free energy functional as well as an additional function (or functions), h, which determines how the membrane is being deformed.

For example, in the case of our SCFT bilayer, we could define the interface as being where $\phi_A(x, y, z) = \phi_B(x, y, z)$. For fixed x, y, there will be two values of z where this relation holds (one for the upper leaflet and one for the lower leaflet). Hence, we could deform the membrane by specifying two functions, $h_\pm(x, y)$, which give the heights of the upper and lower leaflet. The constraints would take the form

$$G_\pm[\phi_A, \phi_B; h_\pm] = \phi_A(x, y, h_\pm(x, y) - \phi_B(x, y, h_\pm(x, y) = 0.$$

We could simplify these constraints to depend on only one field and one parameter function by defining a new field, $\phi = \phi_A - \phi_B$, and assuming that the bilayer has a constant mid-plane height, $h = (h_+ + h_-)/2$, but variable thickness, $t(x, y)$. Then we have the constraints

$$G_\pm[\phi; t] = \phi(x, y, h \pm t(x, y)/2) = 0. \tag{5.1.1}$$

Notice that each $G_\pm$ is indeed an operator as it maps a function of three variables (ϕ) to a function of two variables. The constraint demands that

this function be identically zero. Keep this example constraint in mind as we continue through this calculation.

We can now define a new functional, $f[h]$, as follows:

$$f[h] = F[\phi_*], \tag{5.1.2}$$

where ϕ_* is a solution to the constrained optimization problem

$$\text{Minimize } F[\phi] \text{ subject to } G_i[\phi; h] = 0 \text{ for } i \in \{1, 2, \ldots, n\}. \tag{5.1.3}$$

Thus, the functional $f[h]$ captures the effect deforming the bilayer has on the free energy. Moreover, if we expand f about the flat bilayer then we can directly obtain the mechanical properties of the bilayer in terms of the flat membrane SCFT solution since the coefficients of the expansion will depend on the flat fields and correspond to mechanical properties (such as the bending modulus). To second order, we can write

$$f[h_* + \delta h] = f[h_*] + \left\langle \frac{\delta f}{\delta h}[h_*],\ \delta h \right\rangle + \frac{1}{2}\left\langle \frac{\delta^2 f}{\delta h^2}[h_*]\delta h,\ \delta h \right\rangle, \tag{5.1.4}$$

where h_* corresponds to a flat bilayer and the inner products are the standard function space inner products (i.e. integration). For instance, in the example above, $h_* = 0$ and the inner products would correspond to integration over x and y. Note that in the last term of Equation 5.1.4, $\delta^2 f/\delta h^2$, is an operator which acts on δh (much like how the Hessian of a scalar function of many variables is a matrix). It will be important in what follows to note what type of object results from a functional derivative and it is often helpful to think about the multi-variable calculus analogy. Since (in the case of zero spontaneous curvature) the flat membrane must correspond to a minimum of f (bending the

membrane always costs energy), we must have that $(\delta f/\delta h)[h_*] = 0$. Thus it only remains to compute the second functional derivative of f. For simplicity, from this point forward we will assume that $n = 1$ so that there is only one constraint, $G[\phi; h]$.

In order to perform this calculation, we will begin by rewriting Equation 5.1.3 using a Lagrange multiplier, λ,

$$\frac{\delta}{\delta\phi}\Big(F[\phi] - \langle\lambda,\ G[\phi; h]\rangle\Big) = 0 \tag{5.1.5a}$$

$$G[\phi; h] = 0, \tag{5.1.5b}$$

where λ is a function compatible with the constraint in the sense that the inner product is well defined. For example, using the constraint in Equation 5.1.1, λ would be a function of two variables and the inner product would be integration over x and y. Carrying through the functional derivative in Equation 5.1.5a, we obtain

$$\frac{\delta F}{\delta\phi} - \left(\frac{\delta G}{\delta\phi}\right)^\dagger \lambda = 0, \tag{5.1.6}$$

where the $\left(\frac{\delta G}{\delta\phi}\right)^\dagger$ is the adjoint[a] of the operator $\frac{\delta G}{\delta\phi}$. Combining this equation with the chain rule, we can write the first functional derivative of f as

$$\begin{aligned}\frac{\delta f}{\delta h} &= \left(\frac{\delta\phi_*}{\delta h}\right)^\dagger \frac{\delta F}{\delta\phi}[\phi_*] \\ &= \left(\frac{\delta G}{\delta\phi}[\phi_*]\frac{\delta\phi_*}{\delta h}\right)^\dagger \lambda,\end{aligned} \tag{5.1.7}$$

[a] The adjoint of an operator A is defined by the property that $\langle x,\ Ay\rangle = \langle A^\dagger x,\ y\rangle$ for all $x, y \in H$, where H is a Hilbert space with inner product $\langle\cdot,\ \cdot\rangle$.

where ϕ_* is as in Equation 5.1.2. Note that ϕ_* depends on h implicitly since it solves the constrained optimization problem. We can eliminate $\delta\phi_*/\delta h$ by taking the functional derivative of Equation 5.1.5b with respect to h to obtain

$$\frac{\delta G}{\delta h}[\phi_*] + \frac{\delta G}{\delta \phi}[\phi_*]\frac{\delta \phi_*}{\delta h} = 0. \tag{5.1.8}$$

By substituting Equation 5.1.8 into Equation 5.1.7 we conclude that

$$\frac{\delta f}{\delta h} = -\left(\frac{\delta G}{\delta h}[\phi_*]\right)^\dagger \lambda. \tag{5.1.9}$$

Note that just as ϕ_* implicitly depends on h, so does λ and we have already argued that $(\delta f/\delta h)[h_*] = 0$, hence Equation 5.1.9 allows us to conclude that at $h = h_*$, $\lambda = 0$. This is an important observation since it will greatly simplify future equations. From this point forward we will only be considering $h = h_*$ so that we can ignore any terms which include λ. We will also drop explicit references to ϕ_*, but keep in mind that all functional derivatives are being evaluated at $[\phi_*; h_*]$, i.e. the flat membrane field solutions.

We now want to use Equation 5.1.9 in order to compute the second functional derivative of f. Taking another functional derivative, we have

$$\frac{\delta^2 f}{\delta h^2}[h_*] = -\left(\frac{\delta G}{\delta h}\right)^\dagger \frac{\delta \lambda}{\delta h}. \tag{5.1.10}$$

We can substitute $\delta\lambda/\delta h$ out of Equation 5.1.10 in two steps. First, replace $\delta G/\delta h$ using Equation 5.1.8 to obtain

$$\frac{\delta^2 f}{\delta h^2}[h_*] = \left(\frac{\delta \phi_*}{\delta h}\right)^\dagger \left(\frac{\delta G}{\delta \phi}\right)^\dagger \frac{\delta \lambda}{\delta h}.$$

Second, we take another functional derivative of Equation 5.1.6 in order to replace $(\delta G/\delta\phi)^\dagger(\delta\lambda/\delta h)$ with $(\delta^2 F/\delta\phi^2)(\delta\phi_*/\delta h)$,

$$\frac{\delta^2 f}{\delta h^2}[h_*] = \left(\frac{\delta \phi_*}{\delta h}\right)^\dagger \frac{\delta^2 F}{\delta \phi^2}\frac{\delta \phi_*}{\delta h}. \tag{5.1.11}$$

Next, we use Equation 5.1.8 to isolate $\delta\phi_*/\delta h$

$$\frac{\delta\phi_*}{\delta h} = -\left(\frac{\delta G}{\delta\phi}\right)^{\ddagger}\frac{\delta G}{\delta h} + \left(I - \left(\frac{\delta G}{\delta\phi}\right)^{\ddagger}\frac{\delta G}{\delta\phi}\right)W, \tag{5.1.12}$$

where $\left(\frac{\delta G}{\delta\phi}\right)^{\ddagger}$ is a generalized inverse[b] of the operator $\frac{\delta G}{\delta\phi}$, I is the identity operator and W is an arbitrary operator. Finally, we substitute Equation 5.1.12 in to Equation 5.1.11 to obtain

$$\frac{\delta^2 f}{\delta h^2}[h_*] = \mathcal{G}^\dagger\frac{\delta^2 F}{\delta\phi^2}\mathcal{G} - \mathcal{G}^\dagger\frac{\delta^2 F}{\delta\phi^2}\overline{\mathcal{G}}W - (\overline{\mathcal{G}}W)^\dagger\frac{\delta^2 F}{\delta\phi^2}\mathcal{G} + (\overline{\mathcal{G}}W)^\dagger\frac{\delta^2 F}{\delta\phi^2}(\overline{\mathcal{G}}W) \tag{5.1.13}$$

where $\mathcal{G} = \left(\frac{\delta G}{\delta\phi}\right)^{\ddagger}\frac{\delta G}{\delta h}$ and $\overline{\mathcal{G}} = I - \left(\frac{\delta G}{\delta\phi}\right)^{\ddagger}\frac{\delta G}{\delta\phi}$. Notice that if $\left(\frac{\delta G}{\delta\phi}\right)^{\ddagger}$ is chosen to be a left-inverse of $\frac{\delta G}{\delta\phi}$ then $\overline{\mathcal{G}} = 0$. Therefore, we have shown that for a suitably chosen generalized inverse,

$$f[h_* + \delta h] = f[h_*] + \frac{1}{2}\left\langle\frac{\delta^2 F}{\delta\phi^2}\mathcal{G}\delta h,\ \mathcal{G}\delta h\right\rangle. \tag{5.1.14}$$

5.2 Example Calculation

To illustrate the usefulness of Equation 5.1.14, let us consider a simple example. The Landau free energy functional for a simple liquid-vapour interface is given by [67]

$$F[\phi] = \int d\mathbf{r}\ \left(g(\phi) + \frac{1}{2}k\left\|\nabla\phi\right\|^2\right), \tag{5.2.1}$$

where ϕ is the single particle density, $g(\phi)$ is the free energy per unit volume of a fluid with density ϕ, and $k > 0$ is a constant which parametrizes the

[b] The generalized inverse of an operator A is defined by the property $AA^\ddagger A = A$. One can prove that $\left(A^\dagger\right)^\ddagger = \left(A^\ddagger\right)^\dagger$, so we will denote both adjoint of the generalized inverse and generalized inverse of the adjoint as $A^{\dagger\ddagger}$.

cost of forming an interface. The free energy density, $g(\phi)$ is assumed to have a double-well structure with the two minima corresponding to the liquid and vapour phases. We will assume that the system is tuned for co-existence of the two phases so that the value of g at each of those minima are equal. We will use Equation 5.1.14 in order to calculate the surface tension of a flat interface formed in this system.

In this example, we will assume that the z-axis is perpendicular to the interface and that $h(x, y)$ gives the height of that interface. Clearly, $h_* = 0$ corresponds to the flat interface. The constraint we use to deform the interface according to the function h is

$$G[\phi, h] = \phi(x, y, h(x, y)) - \overline{\phi} = 0, \tag{5.2.2}$$

where $\overline{\phi}$ is the average single particle density between the liquid and vapour phases (i.e. the density in the middle of the interface). In order to apply Equation 5.1.14 we first need to compute $\delta G/\delta\phi$ and $\delta G/\delta h$. Define the mapping A_h by the rule $\phi(x, y, z) \mapsto \phi(x, y, h(x, y))$. It is clear that in terms of this map, $G[\phi, h] = A_h\phi - \overline{\phi}$, and hence it must be the case that $\delta G/\delta\phi = A_h$. In terms of the Dirac delta function, A_h can be expressed as $A_h\phi = \int dz\ \phi(x, y, z)\delta(z - h(x, y))$. Using this form we can compute $\delta G/\delta h$ with the chain rule and integration by parts

$$\begin{aligned}
\frac{\delta G}{\delta h} &= \frac{\delta}{\delta h}\left(\int dz\ \phi(x, y, z)\delta(z - h(x, y))\right) \\
&= -\int dz\ \phi(x, y, z)\delta'(z - h(x, y)) \\
&= \int dz\ \frac{\partial\phi}{\partial z}\delta(z - h(x, y)) \\
&= A_h\frac{\partial\phi}{\partial z}.
\end{aligned}$$

Next, we compute the operator $\mathcal{G}$,

$$\mathcal{G} = \left(\frac{\delta G}{\delta \phi}\right)^{\ddagger} \frac{\delta G}{\delta h} = A_h^{\ddagger} A_h \frac{\partial \phi}{\partial z} = \frac{\partial \phi}{\partial z},$$

where the last step follows from the fact that in the derivation of Equation 5.1.14 we chose to use a left inverse for the generalized inverse. The final piece we need is that $\delta^2 F/\delta\phi^2 = g''(\phi) - k\nabla^2$; now we are ready to apply the formula. Note that we are evaluating the functional derivatives at the flat profile, ϕ_0, which by symmetry can only depend on z.

$$\begin{aligned} f[\delta h] &= f[\phi_0] + \frac{1}{2}\int dxdydz\ \phi_0'(z)\delta h(x,y)\left[g''(\phi_0) - k\nabla^2\right]\phi_0'(z)\delta h(x,y) \\ &= f[\phi_0] + \frac{1}{2}\int dxdydz\ g''(\phi_0)\left(\phi_0'(z)\delta h(x,y)\right)^2 + k\left\|\nabla(\phi_0'\delta h)\right\|^2 \\ &= f[\phi_0] + \frac{1}{2}\int dxdy\left(\left[\int dz\ g''(\phi_0)(\phi_0')^2 + k(\phi_0'')^2\right]\delta h^2 + \left[k\int dz\ (\phi_0')^2\right]\|\nabla\delta h\|^2\right), \end{aligned}$$

where the second equality follows using integration by parts. Since $\|\nabla\delta h\|^2$ represents the increase in area of the interface due to the deformation, we recognize its coefficient as the surface tension of the interface, γ. Therefore,

$$\gamma = k\int dz\ (\phi_0')^2,$$

which is the same result as that obtained in Ref. [67] by a different method. Also note that the δh^2 coefficient must be zero, by symmetry. We now show this is indeed the case. Since ϕ_0 is the flat density profile it must minimize the free energy functional given in Equation 5.2.1 and therefore must satisfy

$$g'(\phi_0) - k\phi_0'' = 0 \tag{5.2.3}$$

by the Euler-Lagrange equation. Differentiating Equation 5.2.3 with respect to z we see that

$$g''(\phi_0)\phi_0' = k\phi_0'''.$$

Substituting this into the δh^2 coefficient above, we have

$$\begin{aligned}\int dz\ g''(\phi_0)(\phi_0')^2 + k(\phi_0'')^2 &= \int dz\ k\phi'''\phi_0' + k(\phi_0'')^2 \\ &= \int dz\ \ -k(\phi_0'')^2 + k(\phi_0'')^2 \\ &= 0,\end{aligned}$$

where the second last equality follows from integration by parts.

Therefore, we have seen in this example that the theoretical framework developed here has taken the Landau theory defined by the free energy functional given in Equation 5.2.1 and connected it to an elastic theory defined by the free energy functional

$$F[h] = F_0 + \int dxdy\ \gamma \left\|\nabla h\right\|^2, \tag{5.2.4}$$

with $\gamma = k\int dz\ (\phi_0')^2$ and $\phi_0(z)$ the density profile for a flat interface.

5.3 Remarks

With this theoretical framework laid out, one would like extend it to the case of two constraints then derive a formula similar to Equation 5.1.14. Using that new equation, with the SCFT free energy functional and constraints like those in Equation 5.1.1, would create formulas for the mechanical properties of the bilayer in terms of derivatives and integrals of the flat polymer profiles. However, deriving the new formula and then computing each of the pieces involved, as was done in the example above, would require some significant effort beyond the scope of this thesis. Although, that calculation should be done in some future work since the result would be very useful.

Chapter 6

Conclusion

In conclusion, we have used self-consistent field theory (SCFT) to study the morphology of a lipid bilayer near a transmembrane protein. The connection between the biological system and SCFT was made by modelling the lipids as diblock copolymers and the protein as a rigid cylinder. This model framework was also expected to be able to study surface proteins with non-zero spontaneous curvature, however significant future work is required to obtain numerical solutions in this case.

Our calculations have shown that a second order wetting phase transition occurs for strong enough interactions between a very long hydrophobic inclusion and the bilayer membrane. For values of the interaction below the wetting transition, we also verified that an elastic theory of the bilayer thickness is consistent with SCFT. This is true in the sense that they make the same predictions when the same mechanical properties and boundary conditions are used for both (no fitting required). A systematic study of the membrane boundary conditions at the protein interface was also done using our SCFT calculations. In light of the consistency between SCFT and elastic theory, these systematic trends are important as they give guidelines for boundary

conditions used in future studies of bilayers with elastic theory. Indeed, we advocate for the continued use of elastic theories since our work as shown they provide high quality predictions and that fitting elastic theory curves to other data is an accurate way to determine mechanical properties of bilayers.

Additionally, analytical work was done to derive Equation 5.1.14, which can be used to calculate mechanical properties of a system without performing numerical calculations that explicitly deform the system. As an example, we have used this formalism to derive the surface tension of a liquid-vapour interface within Landau theory. This analytical framework, when applied to SCFT, would save significant computational time when determining mechanical properties of polymer systems. Hence, this result is important to the computational polymer physics community as a whole. Although Equation 5.1.14 is not applied to SCFT in this work, we believe the mathematical framework itself is useful and could be applied in future works regarding mechanical properties.

Appendix A

Full SCFT Derivation

Here we present a derivation of the SCFT equations given in subsection 2.2.2, following the works in Refs. [51, 69–72].

Recall the notation from subsection 2.2.2. As some further notation, We will denote the space curve used in the continuous Gaussian chain model for the α-block of the j^{th} chain by $\mathbf{R}_j^{(\alpha)}(s)$.

The α-monomer concentration field for a given chain configuration is thus given by

$$\hat{\phi}_\alpha(\mathbf{r}) = \frac{1}{\rho_0} \sum_{j=1}^{n_p} \int_0^{N_\alpha} \delta\left(\mathbf{r} - \mathbf{R}_j^{(\alpha)}(s)\right)\, ds, \tag{A.1}$$

where $\alpha \in \{A, B\}$ if $p = 1$, $\alpha = C$ if $p = 2$ and $\delta(\mathbf{r})$ is the Dirac delta function on $\mathbb{R}^3$. Using the result from Equation 2.2.2, the probability density for the configuration of a chain of a particular block is

$$p\left[\mathbf{R}_j^{(\alpha)}(s)\right] = A \exp\left(-\frac{3}{2b_\alpha^2} \int_0^{N_\alpha} \left\| \frac{d\mathbf{R}_j^{(\alpha)}}{ds} \right\|^2 ds\right), \tag{A.2}$$

and hence the probability density for a configuration of chains of the entire system, $\{\mathbf{R}_j(s)\}$ is

$$P(\{\mathbf{R}_j(s)\}) = \prod_{j=1}^{n_1} \left(p\left[\mathbf{R}_j^{(A)}(s)\right] p\left[\mathbf{R}_j^{(B)}(s)\right] \delta\left(\mathbf{R}_j^{(A)}(N_A) - \mathbf{R}_j^{(B)}(N_B)\right)\right) \prod_{j=1}^{n_2} \left(p\left[\mathbf{R}_j^{(C)}(s)\right]\right), \tag{A.3}$$

where the Dirac delta function ensures the A- and B-blocks are bonded together. We can hence write the partition function of the system as the functional integral

$$Z = \frac{z_1^{n_1} z_2^{n_2}}{n_1! n_2!} \int \mathcal{D}\{\mathbf{R}_j(s)\} P(\{\mathbf{R}_j(s)\}) \prod_{\mathbf{r}} \delta\left(\sum_{\alpha} \hat{\phi}_\alpha(\mathbf{r}) - 1\right) e^{-W\left[\{\hat{\phi}_\alpha(\mathbf{r})\}\right]}, \tag{A.4}$$

where z_p, $p \in \{1, 2\}$ are the partition functions of a polymer chain due to kinetic energy, $\{\hat{\phi}_\alpha(\mathbf{r})\}$ is short-hand for $\{\hat{\phi}_\alpha(\mathbf{r})\}_{\alpha \in \{A,B,C\}}$ (i.e. it is the set of concentration fields from all types of monomers), $W\left[\{\hat{\phi}_\alpha(\mathbf{r})\}\right] = V\left[\{\hat{\phi}_\alpha(\mathbf{r})\}\right]/(k_B T)$ is the intermolecular potential functional and the Dirac delta function ensures incompressibility which is meant to model the hardcore interactions of the polymers. Recall from subsection 2.2.2 that the Flory-Huggins parameter models the interaction between the monomers, hence the intermolecular potential functional has the form

$$W\left[\{\hat{\phi}_\alpha(\mathbf{r})\}\right] = \frac{1}{2} \sum_{\alpha \neq \beta} \rho_0 \chi_{\alpha\beta} \int \hat{\phi}_\alpha(\mathbf{r}) \hat{\phi}_\beta(\mathbf{r}) \, d\mathbf{r}. \tag{A.5}$$

To avoid integrating over the chain configurations themselves we can rewrite the partition function as

$$\begin{aligned} Z = \tfrac{z_1^{n_1} z_2^{n_2}}{n_1! n_2!} \int \mathcal{D}\{\phi_\alpha\} \mathcal{D}\{\omega_\alpha\} \textstyle\prod_{\mathbf{r}} \delta\left(\sum_\alpha \phi_\alpha(\mathbf{r}) - 1\right) \exp\left(\sum_\alpha \rho_0 \int \omega_\alpha(\mathbf{r}) \phi_\alpha(\mathbf{r}) \, d\mathbf{r} - W\left[\{\phi_\alpha(\mathbf{r})\}\right]\right) \\ \times \int \mathcal{D}\{\mathbf{R}_j(s)\} P(\{\mathbf{R}_j(s)\}) \exp\left(-\textstyle\sum_\alpha \rho_0 \int \omega_\alpha(\mathbf{r}) \hat{\phi}_\alpha(\mathbf{r}) \, d\mathbf{r}\right), \end{aligned} \tag{A.6}$$

where we have used the identity

$$1 = \int \mathcal{D}\{\phi_\alpha\} \prod_{\alpha} \prod_{\mathbf{r}} \delta\left(\phi_\alpha(\mathbf{r}) - \hat{\phi}_\alpha(\mathbf{r})\right) \tag{A.7}$$

and the integral definition of the Dirac delta function,
$\delta(x - x_0) = \int_{-\infty}^{\infty} \exp(2\pi i k(x - x_0))\ dk$ to introduce auxiliary fields, $\omega_\alpha(\mathbf{r})$, in order to write the identity as

$$1 = \int \mathcal{D}\{\phi_\alpha\}\mathcal{D}\{\omega_\alpha\} \exp\left(\sum_\alpha \rho_0 \int \omega_\alpha(\mathbf{r})(\phi_\alpha(\mathbf{r}) - \hat{\phi}_\alpha(\mathbf{r}))\ d\mathbf{r}\right), \tag{A.8}$$

where the factor ρ_0 was introduced for convenience by scaling the ω_α fields and the range of the $\{\omega_\alpha\}$ functional integral varies the value of each $\omega_\alpha(\mathbf{r})$ over a line in the complex plane from $-i\infty$ to $i\infty$. We can rewrite the latter term in Equation A.6 as $(\mathcal{Q}_1 V)^{n_1}(\mathcal{Q}_2 V)^{n_2}$, where $\mathcal{Q}_p\left[\{\omega_\alpha(\mathbf{r})\}\right]$, $\alpha \in \{A, B\}$ if $p = 1$ and $\alpha = C$ if $p = 2$, are the partition functions of a polymer chain in the external fields ω_α. These single-chain partition functions are defined by the path integrals

$$\mathcal{Q}_1\left[\{\omega_\alpha(\mathbf{r})\}\right] = \frac{1}{V}\int \mathcal{D}\mathbf{R}_j^{(A)}\mathcal{D}\mathbf{R}_j^{(B)}\ p\left[\mathbf{R}_j^{(A)}(s)\right] p\left[\mathbf{R}_j^{(B)}(s)\right] \delta\left(\mathbf{R}_j^{(A)}(N_A) - \mathbf{R}_j^{(B)}(N_B)\right) \times \exp\left(-\sum_{\alpha\in\{A,B\}} \int_0^{N_\alpha} \omega_\alpha\left(\mathbf{R}_j^{(\alpha)}(s)\right)\ ds\right) \tag{A.9}$$

$$\mathcal{Q}_2\left[\omega_C(\mathbf{r})\right] = \frac{1}{V}\int \mathcal{D}\mathbf{R}_j^{(C)}\ p\left[\mathbf{R}_j^{(C)}(s)\right] \exp\left(-\int_0^{N_C} \omega_C\left(\mathbf{R}_j^{(C)}(s)\right)\ ds\right). \tag{A.10}$$

The expressions become more manageable be defining chain propagators,

$$Q_\alpha(\mathbf{r}, s|\mathbf{r}') = \int_{\mathbf{R}(0)=\mathbf{r}'}^{\mathbf{R}(s)=\mathbf{r}} \mathcal{D}\mathbf{R}\ \exp\left(-\int_0^{N_\alpha} \frac{3}{2b_\alpha^2}\left\|\frac{d\mathbf{R}}{dt}\right\|^2 + \omega_\alpha\left(\mathbf{R}(t)\right)\ dt\right), \tag{A.11}$$

where $\alpha \in \{A, B, C\}$. Physically, we interpret $Q_\alpha(\mathbf{r}, s|\mathbf{r}')$ as the probability density for monomer s being at position $\mathbf{r}$ given that monomer 0 is at $\mathbf{r}'$ in the

presence of an external field ω_α. One can show that these propagators satisfy the differential equation

$$\frac{\partial}{\partial s}Q_\alpha = \frac{b_\alpha^2}{6}\nabla^2 Q_\alpha - \omega_\alpha Q_\alpha, \tag{A.12}$$

with the initial condition $Q_\alpha(\mathbf{r}, 0|\mathbf{r}') = \delta(\mathbf{r} - \mathbf{r}')$. In terms of the propagators, the single-chain partition functions become

$$\mathcal{Q}_1\left[\{\omega_\alpha(\mathbf{r})\}\right] = \frac{1}{V}\int Q_A(\mathbf{r}_1, N_A|\mathbf{r}_2)Q_B(\mathbf{r}_1, N_B|\mathbf{r}_3)\ d\mathbf{r}_1 d\mathbf{r}_2 d\mathbf{r}_3 \tag{A.13}$$

$$\mathcal{Q}_2\left[\omega_C(\mathbf{r})\right] = \frac{1}{V}\int Q_C(\mathbf{r}_1, N_C|\mathbf{r}_2)\ d\mathbf{r}_1 d\mathbf{r}_2. \tag{A.14}$$

As one further simplification we can introduce the end-integrated propagators,

$$q_\alpha(\mathbf{r}, s) = \int Q_\alpha(\mathbf{r}, s|\mathbf{r}')\ d\mathbf{r}' \tag{A.15}$$

$$q_\alpha^\dagger(\mathbf{r}, s) = \int Q_\alpha(\mathbf{r}, s|\mathbf{r}')Q_\beta(\mathbf{r}, N_\beta|\mathbf{r}'')\ d\mathbf{r}' d\mathbf{r}'' \tag{A.16}$$

$$q_C = \int Q_C(\mathbf{r}, s|\mathbf{r}')\ d\mathbf{r}', \tag{A.17}$$

where if $\alpha = A$ then $\beta = B$ and vice versa. These end-integrated propagators also satisfy Equation A.12, with the initial conditions

$$q_\alpha(\mathbf{r}, 0) = 1 \tag{A.18}$$

$$q_\alpha^\dagger(\mathbf{r}, 0) = \int Q_\beta(\mathbf{r}, N_\beta|\mathbf{r}')\ d\mathbf{r}' = q_\beta(\mathbf{r}, N_\beta) \tag{A.19}$$

$$q_C(\mathbf{r}, 0) = 1. \tag{A.20}$$

With these definitions, the single-chain partition functions are given by

$$\mathcal{Q}_1\left[\{\omega_\alpha\}\right] = \frac{1}{V}\int q_A^\dagger(\mathbf{r}, N_A)\ d\mathbf{r} = \frac{1}{V}\int q_B^\dagger(\mathbf{r}, N_B)\ d\mathbf{r} \tag{A.21}$$

$$\mathcal{Q}_2\left[\omega_C\right] = \frac{1}{V}\int q_C(\mathbf{r}, N_C)\ d\mathbf{r} \tag{A.22}$$

and the partition function can be written as

$$Z = \int \mathcal{D}\{\phi_\alpha\}\mathcal{D}\{\omega_\alpha\}\mathcal{D}\eta \times \exp\left(\sum_\alpha \rho_0 \int \omega_\alpha(\mathbf{r})\phi_\alpha(\mathbf{r})\ d\mathbf{r} - W\left[\{\phi_\alpha\}\right] - \rho_0 \int \eta(\mathbf{r}) \left(\sum_\alpha \phi_\alpha(\mathbf{r}) - 1\right)\ d\mathbf{r}\right) \times \frac{(z_1\mathcal{Q}_1 V)^{n_1}}{n_1!}\frac{(z_2\mathcal{Q}_2 V)^{n_2}}{n_2!}, \tag{A.23}$$

where the field $\eta(\mathbf{r})$ has replaced the Dirac delta function enforcing incompressibility.

We shall now assume that we are considering a canonical ensemble, then the number of polymer chains in the volume (and hence also the average concentrations given by Equation 2.2.3) are constant. We can then write the partition function as

$$Z = \int \mathcal{D}\{\phi_\alpha\}\mathcal{D}\{\omega_\alpha\}\mathcal{D}\eta \exp\left(-\rho_0 \int \eta(\mathbf{r}) \left(\sum_\alpha \phi_\alpha(\mathbf{r}) - 1\right)\ d\mathbf{r}\right) e^{-F[\{\phi_\alpha\},\{\omega_\alpha\}]}, \tag{A.24}$$

where

$$F\left[\{\phi_\alpha\},\{\omega_\alpha\}\right] = W\left[\{\phi_\alpha\}\right] - \sum_\alpha \rho_0 \int \omega_\alpha(\mathbf{r})\phi_\alpha(\mathbf{r})\ d\mathbf{r} - \ln\left(\frac{(z_1\mathcal{Q}_1 V)^{n_1}}{n_1}\right) - \ln\left(\frac{(z_2\mathcal{Q}_2 V)^{n_2}}{n_2}\right) \tag{A.25}$$

is the free energy functional. Notice that up to this point no explicit length scale has been specified. Adopting the radius of gyration length scale defined earlier and using the definition of the average polymer concentrations the free energy functional becomes

$$F\left[\{\phi_\alpha\},\{\omega_\alpha\}\right] = \frac{\rho R_g^3 V}{N}\left(\frac{1}{V}\int \frac{1}{2}\sum_{\alpha\neq\beta}\chi_{\alpha\beta}N\phi_\alpha(\mathbf{r})\phi_\beta(\mathbf{r}) - \sum_\alpha N\omega_\alpha(\mathbf{r})\phi_\alpha(\mathbf{r})\ d\mathbf{r} - \sum_p \frac{\overline{\phi_p}}{\kappa_p}\ln\left(\frac{z_p e N_p \mathcal{Q}_p}{\rho_0 \overline{\phi_p}}\right)\right), \tag{A.26}$$

where we have also used the Stirling approximation $n! \approx (n/e)^n$ to simplify the logarithm terms. We can then define a free energy density,

$$f\left[\{\phi_\alpha\},\{\omega_\alpha\}\right] \equiv \frac{N}{\rho_0 R_g^3 V} F\left[\{\phi_\alpha\},\{\omega_\alpha\}\right]. \tag{A.27}$$

We can also write Equation A.12 in a dimensionless form in this length scale since $b_\alpha^2/6 = R_g^2\sigma_\alpha^2/N$,

$$N\frac{\partial}{\partial s}Q_\alpha = R_g^2\sigma_\alpha^2\nabla^2 Q_\alpha - N\omega_\alpha Q_\alpha. \tag{A.28}$$

We can eliminate additional factors of N by scaling the arclength of the polymers in units of N and redefining the ω_α fields to include the factor, $N\omega_\alpha \to \omega_\alpha$. In this scaled form the end-integrated propagators satisfy,

$$\frac{\partial q_\alpha}{\partial s} = \sigma_\alpha^2\nabla^2 q_\alpha - \omega_\alpha q_\alpha,\ \alpha \in \{A,B,C\} \tag{A.29}$$

$$q_\alpha(\mathbf{r},0) = 1 \tag{A.30}$$

$$\frac{\partial q_\alpha^\dagger}{\partial s} = \sigma_\alpha^2\nabla^2 q_\alpha^\dagger - \omega_\alpha q_\alpha^\dagger,\ \alpha \in \{A,B\} \tag{A.31}$$

$$q_\alpha^\dagger(\mathbf{r},0) = q_\beta(\mathbf{r},f_\beta),\ \beta \neq \alpha \tag{A.32}$$

and the free energy density is

$$f\left[\{\phi_\alpha\},\{\omega_\alpha\}\right] = \frac{1}{V}\int\left(\frac{1}{2}\sum_{\alpha\neq\beta}\chi_{\alpha\beta}N\phi_\alpha(\mathbf{r})\phi_\beta(\mathbf{r}) - \sum_\alpha \omega_\alpha(\mathbf{r})\phi_\alpha(\mathbf{r})\right)d\mathbf{r} - \sum_p \frac{\overline{\phi_p}}{\kappa_p}\ln\mathcal{Q}_p, \tag{A.33}$$

where some constants have been dropped as they can be viewed as constant terms in the $\omega_\alpha(\mathbf{r})$ fields and hence ignored since adding a constant to a field does not change the physics. Finally, we define the effective free energy

$$\Omega\left[\{\phi_\alpha\},\{\omega_\alpha\},\eta\right] = \rho_0 R_g^3\left(\frac{V}{N}f\left[\{\phi_\alpha\},\{\omega_\alpha\}\right] + \int\eta(\mathbf{r})\left(\sum_\alpha\phi_\alpha(\mathbf{r}) - 1\right)d\mathbf{r}\right) \tag{A.34}$$

and write the partition function as

$$Z = \int \mathcal{D}\{\phi_\alpha\}\mathcal{D}\{\omega_\alpha\}\mathcal{D}\eta \; e^{-\Omega[\{\phi_\alpha\},\{\omega_\alpha\},\eta]}. \tag{A.35}$$

In general, direct evaluation of the partition function is not possible (functional integrals can be very difficult to compute and sometimes even diverge!). To use the expressions we have derived we apply the mean field approximation which formally is a saddle–point approximation to the functional integral and so we require first order variations of the integrand to vanish,

$$\frac{\delta\Omega}{\delta\phi_\alpha} = \frac{\delta\Omega}{\delta\omega_\alpha} = \frac{\delta\Omega}{\delta\eta} = 0. \tag{A.36}$$

This requirement leads to the mean field equations

$$\phi_\alpha(\mathbf{r}) = \frac{\overline{\phi_1}}{\mathcal{Q}_1}\int_0^{f_\alpha} q_\alpha(\mathbf{r},s)q_\alpha^\dagger(\mathbf{r},f_\alpha - s)\; ds,\;\; \alpha \in \{A,B\} \tag{A.37}$$

$$\phi_C(\mathbf{r}) = \frac{\overline{\phi_2}}{\kappa_2\mathcal{Q}_2}\int_0^{\kappa_2} q_C(\mathbf{r},s)q_C(\mathbf{r},\kappa_2 - s)\; ds \tag{A.38}$$

$$\omega_\alpha(\mathbf{r}) = \sum_{\alpha\neq\beta}\chi_{\alpha\beta}N\left(\phi_\beta(\mathbf{r}) - \overline{\phi_\beta}\right) + \eta(\mathbf{r}) \tag{A.39}$$

$$\sum_{\alpha\in\{A,B,C\}} \phi_\alpha(\mathbf{r}) = 1, \tag{A.40}$$

where the constants

$$\overline{\phi_A} = \overline{\phi_1}f_A, \qquad \overline{\phi_B} = \overline{\phi_1}f_B, \qquad \overline{\phi_C} = \overline{\phi_2}$$

were added the $\omega_\alpha(\mathbf{r})$ fields to make $\int \omega_\alpha(\mathbf{r})\; d\mathbf{r} = 0$. We now see the physical meaning of the $\omega_\alpha(\mathbf{r})$ field is the effective potential felt by an α-block at position $\mathbf{r}$ and so captures the interaction between polymers without explicitly tracking the positions of each polymer strand. The field $\eta(\mathbf{r})$ can also be viewed as a Lagrange multiplier to enforce the incompressibility condition.

Appendix B

The ADI Method

Here we present the Alternating Direction Implicit (ADI) method in detail. In what follows the notation introduced in subsection 3.2.2 is used. For simplicity of the presentation we set $\sigma = 1$.

The ADI method numerically evolves the solution forward from the initial condition $q(\mathbf{r}, 0)$ to $q(\mathbf{r}, 1)$ (here we are using the contour variable which is scaled by N) in half steps. First, keeping the z part of the differential operator fixed at s_k while advancing the r differential operator to $s_{k+1/2}$, we have

$$\frac{q_{i,j}^{k+1/2} - q_{i,j}^{k}}{(\Delta s/2)} = \left(\delta_r^2 q_{i,j}^{k+1/2} + \frac{1}{r_i}\delta_r q_{i,j}^{k+1/2} + \delta_z^2 q_{i,j}^{k}\right) - \omega_{i,j}\frac{(q_{i,j}^{k+1/2} + q_{i,j}^{k})}{2}. \quad \text{(B.41)}$$

Notice that the field term is averaged between the two contour steps. Collecting the $s_{k+1/2}$ step terms together we get

$$\alpha_1 q_{i+1,j}^{k+1/2} + \alpha_0 q_{i,j}^{k+1/2} + \alpha_{-1} q_{i-1,j}^{k+1/2} = \beta_1 q_{i,j+1}^{k} + \beta_0 q_{i,j}^{k} + \beta_{-1} q_{i,j-1}^{k}, \quad \text{(B.42)}$$

where

$$\alpha_1 \equiv -\frac{\Delta s}{2(\Delta r)^2} - \frac{1}{r_i}\frac{\Delta s}{4\Delta r} \quad \text{(B.43)}$$

$$\alpha_0 \equiv 1 + \frac{\Delta s}{(\Delta r)^2} + \frac{\Delta s}{4}\omega_{i,j} \quad \text{(B.44)}$$

$$\alpha_{-1} \equiv -\frac{\Delta s}{2(\Delta r)^2} + \frac{1}{r_i}\frac{\Delta s}{4\Delta r} \quad \text{(B.45)}$$

$$\beta_1 \equiv \frac{\Delta s}{2(\Delta z)^2} \tag{B.46}$$

$$\beta_0 \equiv 1 - \frac{\Delta s}{(\Delta z)^2} - \frac{\Delta s}{4}\omega_{i,j} \tag{B.47}$$

$$\beta_{-1} \equiv \frac{\Delta s}{2(\Delta z)^2}. \tag{B.48}$$

The expression are not well defines on the boundaries $i = 1$, $j = 1$, $i = N_r$, and $j = N_z$ since $i \pm 1$ or $j \pm 1$ falls out off bounds of the lattice. However, the boundary conditions handle these cases. For example, in our implementation we use Neumann boundary conditions, i.e.

$$\left.\frac{\partial q(r,z,s)}{\partial r}\right|_{r=r_{\min},r_{\max}} = \left.\frac{\partial q(r,z,s)}{\partial z}\right|_{z=z_{\min},z_{\max}} = 0. \tag{B.49}$$

On the discrete lattice this corresponds to the relations

$$q^k_{0,j} = q^k_{2,j} \qquad q^k_{i,0} = q^k_{i,2} \tag{B.50}$$

$$q^k_{N_r+1,j} = q^k_{N_r-1,j} \qquad q^k_{i,N_z+1} = q^k_{i,N_z-1}. \tag{B.51}$$

Hence, we can write the system of equations defined by Equation B.42 as the matrix equations:

$$\begin{bmatrix} \alpha_0 & (\alpha_1+\alpha_{-1}) & 0 & \cdots & 0 \\ \alpha_{-1} & \alpha_0 & \alpha_1 & \cdots & 0 \\ \vdots & \ddots & \ddots & \ddots & \vdots \\ 0 & \cdots & \alpha_{-1} & \alpha_0 & \alpha_1 \\ 0 & \cdots & 0 & (\alpha_1+\alpha_{-1}) & \alpha_0 \end{bmatrix} \begin{bmatrix} q^{k+1/2}_{1,1} \\ q^{k+1/2}_{2,1} \\ \vdots \\ q^{k+1/2}_{N_r-1,1} \\ q^{k+1/2}_{N_r,1} \end{bmatrix} = \begin{bmatrix} (\beta_1+\beta_{-1})q^k_{1,2} + \beta_0 q^k_{0,1} \\ (\beta_1+\beta_{-1})q^k_{2,2} + \beta_0 q^k_{1,1} \\ \vdots \\ (\beta_1+\beta_{-1})q^k_{N_r-1,2} + \beta_0 q^k_{N_r-1,1} \\ (\beta_1+\beta_{-1})q^k_{N_r,2} + \beta_0 q^k_{N_r,1} \end{bmatrix}$$

when $j = 1$,

$$\begin{bmatrix} \alpha_0 & (\alpha_1+\alpha_{-1}) & 0 & \cdots & 0 \\ \alpha_{-1} & \alpha_0 & \alpha_1 & \cdots & 0 \\ \vdots & \ddots & \ddots & \ddots & \vdots \\ 0 & \cdots & \alpha_{-1} & \alpha_0 & \alpha_1 \\ 0 & \cdots & 0 & (\alpha_1+\alpha_{-1}) & \alpha_0 \end{bmatrix} \begin{bmatrix} q_{1,j}^{k+1/2} \\ q_{2,j}^{k+1/2} \\ \vdots \\ q_{N_r-1,j}^{k+1/2} \\ q_{N_r,j}^{k+1/2} \end{bmatrix} = \begin{bmatrix} \beta_1 q_{1,j+1}^k + \beta_0 q_{0,j}^k + \beta_{-1} q_{1,j-1}^k \\ \beta_1 q_{2,j+1}^k + \beta_0 q_{1,j}^k + \beta_{-1} q_{2,j-1}^k \\ \vdots \\ \beta_1 q_{N_r-1,j+1}^k + \beta_0 q_{N_r-1,j}^k + \beta_{-1} q_{N_r-1,j-1}^k \\ \beta_1 q_{N_r,j+1}^k + \beta_0 q_{N_r,j}^k + \beta_{-1} q_{N_r,j-1}^k \end{bmatrix}$$

when $2 \leq j \leq N_z - 1$ and

$$\begin{bmatrix} \alpha_0 & (\alpha_1+\alpha_{-1}) & 0 & \cdots & 0 \\ \alpha_{-1} & \alpha_0 & \alpha_1 & \cdots & 0 \\ \vdots & \ddots & \ddots & \ddots & \vdots \\ 0 & \cdots & \alpha_{-1} & \alpha_0 & \alpha_1 \\ 0 & \cdots & 0 & (\alpha_1+\alpha_{-1}) & \alpha_0 \end{bmatrix} \begin{bmatrix} q_{1,N_z}^{k+1/2} \\ q_{2,N_z}^{k+1/2} \\ \vdots \\ q_{N_r-1,N_z}^{k+1/2} \\ q_{N_r,N_z}^{k+1/2} \end{bmatrix} = \begin{bmatrix} (\beta_1+\beta_{-1}) q_{1,N_z-1}^k + \beta_0 q_{0,N_z}^k \\ (\beta_1+\beta_{-1}) q_{2,N_z-1}^k + \beta_0 q_{1,N_z}^k \\ \vdots \\ (\beta_1+\beta_{-1}) q_{N_r-1,N_z-1}^k + \beta_0 q_{N_r-1,N_z}^k \\ (\beta_1+\beta_{-1}) q_{N_r,N_z-1}^k + \beta_0 q_{N_r,N_z}^k \end{bmatrix}$$

when $j = N_z$. These systems of equations can be solved using the tridiagonal matrix algorithm (TDMA), also known as the Thomas algorithm [63, 64]. The TDMA is a matrix inversion procedure which is computationally much faster than simple Gaussian elimination. This speed up with the matrix inversion while maintaining the accuracy of implicitly defining the next contour step is the major advantage to the ADI method.

We can now use the solutions ($q^{s+1/2}$) as the initial conditions for the second step of the ADI method. The derivation for this is the same as above,

however we are now leaving the r part of the differential operator at $s_{k+1/2}$ and incrementing the z part to s_{k+1}. This gives the following system of equations:

$$\gamma_1 q_{i,j+1}^{k+1} + \gamma_0 q_{i,j}^{k+1} + \gamma_{-1} q_{i,j-1}^{k+1} = \sigma_1 q_{i+1,j}^{k+1/2} + \sigma_0 q_{i,j}^{k+1/2} + \sigma_{-1} q_{i-1,j}^{k+1/2} \tag{B.52}$$

with the coefficients on the left hand side defined as

$$\gamma_1 = -\frac{\Delta s}{2(\Delta z)^2} \tag{B.53}$$

$$\gamma_0 = 1 + \frac{\Delta s}{(\Delta z)^2} + \frac{\Delta s}{4}\omega_{i,j} \tag{B.54}$$

$$\gamma_{-1} = -\frac{\Delta s}{2(\Delta z)^2} \tag{B.55}$$

and on right hand side,

$$\sigma_1 = \frac{\Delta s}{2(\Delta r)^2} + \frac{1}{r_i}\frac{\Delta s}{4\Delta r} \tag{B.56}$$

$$\sigma_0 = 1 - \frac{\Delta s}{(\Delta r)^2} - \frac{\Delta s}{4}\omega_{i,j} \tag{B.57}$$

$$\sigma_{-1} = \frac{\Delta s}{2(\Delta r)^2} - \frac{1}{r_i}\frac{\Delta s}{4\Delta r}. \tag{B.58}$$

Setting up matrix equations similar to the previous step and applying the TDMA, completes the step to s_{k+1}. This process is the repeated from s_0 to s_{N_s}, giving the full solution to the PDE.

Bibliography

[1] D. Voet, J. Voet, and C. Pratt, *Fundamentals of Biochemistry: Life at the Molecular Level, 4th Edition: Life at the Molecular Level* (Wiley, 2011).

[2] P. L. Luisi, P. Walde, and T. Oberholzer, Current Opinion in Colloid & Interface Science **4**, 33 (1999).

[3] M. M. Hanczyc and J. W. Szostak, Current Opinion in Chemical Biology **8**, 660 (2004).

[4] G. L. Nicolson, Biochimica et Biophysica Acta (BBA) - Biomembranes Membrane Structure and Function: Relevance in the Cell's Physiology, Pathology and Therapy, **1838**, 1451 (2014).

[5] W. Dowhan, Annual Review of Biochemistry **66**, 199 (1997).

[6] P. R. Cullis and B. de Kruijff, Biochim. Biophys. Acta **559**, 399 (1979).

[7] G. van Meer, D. R. Voelker, and G. W. Feigenson, Nat Rev Mol Cell Biol **9**, 112 (2008).

[8] A. Callan-Jones and P. Bassereau, Current Opinion in Solid State and Materials Science Membrane spatial organization, shape, and remodeling: Materials science and biology, **17**, 143 (2013).

[9] V. A. Frolov, A. V. Shnyrova, and J. Zimmerberg, Cold Spring Harb Perspect Biol **3**, a004747 (2011).

[10] A. G. Lee, Biochimica et Biophysica Acta (BBA) - Biomembranes Lipid-Protein Interactions, **1666**, 62 (2004).

[11] O. Ces and X. Mulet, Signal Transduction **6**, 112 (2006).

[12] C. L. Armstrong, E. Sandqvist, and M. C. Rheinstaedter, Protein Pept. Lett. **18**, 344 (2011).

[13] P. B. Canham, Journal of Theoretical Biology **26**, 61 (1970).

[14] W. Helfrich, Z Naturforsch C **28**, 693 (1973).

[15] E. A. Evans, Biophys J **14**, 923 (1974).

[16] Z. C. Ou-Yang and Z. C. Tu, Int. J. Mod. Phys. B **28**, 1330022 (2013).

[17] P. Bassereau, B. Sorre, and A. Lvy, Advances in Colloid and Interface Science Special issue in honour of Wolfgang Helfrich, **208**, 47 (2014).

[18] J. Li, K. A. Pastor, A.-C. Shi, F. Schmid, and J. Zhou, Phys. Rev. E **88**, 012718 (2013).

[19] R. Tourdot, R. Bradley, N. Ramakrishnan, and R. Radhakrishnan, IET Systems Biology **8**, 198 (2014).

[20] B. Alberts, *Molecular Biology of the Cell: Reference edition* (Garland Science, 2008).

[21] L. E. Cybulski and D. Mendoza, Current Protein & Peptide Science **12**, 760 (2011).

[22] D. A. Hicks, N. N. Nalivaeva, and A. J. Turner, Frontiers in Physiology **3** (2012), 10.3389/fphys.2012.00189.

[23] J. A. Killian, Biochimica et Biophysica Acta **1376**, 401 (1998).

[24] S. K. Kandasamy and R. G. Larson, Biophysical Journal **90**, 2326 (2006).

[25] H. T. McMahon and E. Boucrot, J Cell Sci **128**, 1065 (2015).

[26] H. T. McMahon and J. L. Gallop, Nature **438**, 590 (2005).

[27] A. Zemel, A. Ben-Shaul, and S. May, J. Phys. Chem. B **112**, 6988 (2008).

[28] G. Drin and B. Antonny, FEBS Letters Frontiers in Membrane Biochemistry, **584**, 1840 (2010).

[29] T. Yue, S. Li, X. Zhang, and W. Wang, Soft Matter **6**, 6109 (2010).

[30] B. Antonny, Annual Review of Biochemistry **80**, 101 (2011).

[31] T. Baumgart, B. R. Capraro, C. Zhu, and S. L. Das, Annual Review of Physical Chemistry **62**, 483 (2011).

[32] Y. Rao and V. Haucke, Cell. Mol. Life Sci. **68**, 3983 (2011).

[33] Q. Cui, L. Zhang, Z. Wu, and A. Yethiraj, Current Opinion in Solid State and Materials Science Membrane spatial organization, shape, and remodeling: Materials science and biology, **17**, 164 (2013).

[34] M. M. Kozlov, F. Campelo, N. Liska, L. V. Chernomordik, S. J. Marrink, and H. T. McMahon, Curr. Opin. Cell Biol. **29**, 53 (2014).

[35] S. Suetsugu, S. Kurisu, and T. Takenawa, Physiological Reviews **94**, 1219 (2014).

[36] R. Bradley and R. Radhakrishnan, Polymers **5**, 890 (2013).

[37] M. G. J. Ford, I. G. Mills, B. J. Peter, Y. Vallis, G. J. K. Praefcke, P. R. Evans, and H. T. McMahon, Nature **419**, 361 (2002).

[38] M. Chavent, A. L. Duncan, and M. S. Sansom, Current Opinion in Structural Biology **40**, 8 (2016).

[39] B. West, F. L. H. Brown, and F. Schmid, Biophysical Journal **96**, 101 (2009).

[40] R. Tjörnhammar and O. Edholm, Chemistry and Physics of Lipids Computational approaches to understanding lipid-protein interactions, **169**, 2 (2013).

[41] S. May, Langmuir **18**, 6356 (2002).

[42] S. Mondal, G. Khelashvili, and H. Weinstein, Biophysical Journal **106**, 2305 (2014).

[43] R. W. Tourdot, N. Ramakrishnan, and R. Radhakrishnan, Phys. Rev. E **90**, 022717 (2014).

[44] X.-j. Li and M. Schick, Biophysical Journal **78**, 34 (2000).

[45] F. A. M. Leermakers, A. L. Rabinovich, and N. K. Balabaev, Phys. Rev. E **67**, 011910 (2003).

[46] M. Müller, K. Katsov, and M. Schick, Physics Reports **434**, 113 (2006).

[47] R. A. Kik, F. a. M. Leermakers, and J. M. Kleijn, Phys. Chem. Chem. Phys. **7**, 1996 (2005).

[48] P. G. de Gennes, Rev. Mod. Phys. **57**, 827 (1985).

[49] S. M. Engels and F. a. M. Leermakers, The Journal of Chemical Physics **114**, 4267 (2001).

[50] A. Dehghan, K. A. Pastor, and A.-C. Shi, Phys. Rev. E **91**, 022713 (2015).

[51] G. Fredrickson, *The Equilibrium Theory of Inhomogeneous Polymers*, International Series of Monographs on Physics (OUP Oxford, 2013).

[52] M. W. Matsen, The Journal of Chemical Physics **110**, 4658 (1999).

[53] T. L. Chantawansri, S.-M. Hur, C. J. Garca-Cervera, H. D. Ceniceros, and G. H. Fredrickson, The Journal of Chemical Physics **134**, 244905 (2011).

[54] S. W. Sides, B. J. Kim, E. J. Kramer, and G. H. Fredrickson, Phys. Rev. Lett. **96**, 250601 (2006).

[55] C. W. Wolgemuth and S. X. Sun, Phys. Rev. Lett. **97**, 248101 (2006).

[56] S. Choe and S. X. Sun, The Journal of Chemical Physics **122**, 244912 (2005).

[57] Z. C. Tu and Z. C. Ou-Yang, Journal of Computational and Theoretical Nanoscience **5**, 422 (2008).

[58] A. Granas and J. Dugundji, *Fixed Point Theory*, Springer Monographs in Mathematics (Springer New York, 2013).

[59] D. G. Anderson, J. ACM **12**, 547 (1965).

[60] K.-C. Ng, The Journal of Chemical Physics **61**, 2680 (1974).

[61] M. W. Matsen, Eur. Phys. J. E **30**, 361 (2009).

[62] D. Peaceman and J. H.H. Rachford, Journal for the Society of Industrial and Applied Mathematics **3**, 28 (1955).

[63] L. Thomas, Watson Sci. Comput. Lab. Rept., Columbia University,New York (1949).

[64] G. Bruce, D. Peaceman, H. Rachford, and J. Rice, Trans. Am. Inst. Min. Engrs (Petrol Div.) **198**, 79 (1953).

[65] G. Tzeremes, K. O. Rasmussen, T. Lookman, and A. Saxena, Phys. Rev. E **65**, 041806 (2002).

[66] G. Corliss, C. Faure, A. Griewank, L. Hascoet, and U. Naumann, *Automatic Differentiation of Algorithms: From Simulation to Optimization* (Springer New York, 2013).

[67] M. P. A. Fisher and M. Wortis, Phys. Rev. B **29**, 6252 (1984).

[68] M. Laradji and R. C. Desai, The Journal of Chemical Physics **108**, 4662 (1998).

[69] M. D. Whitmore and J. D. Vavasour, Acta Polymerica **46**, 341 (1995).

[70] F. Schmid, Journal of Physics: Condensed Matter **10**, 8105 (1998).

[71] M. W. Matsen, Journal of Physics: Condensed Matter **14**, R21 (2002).

[72] A.-C. Shi, *Developments in Block Copolymer Science and Technology* (Wiley, 2004) pp. 265–293, edited by I. W. Hamley.